lubricants

MDPI

Review

Research Progress of High-Speed Wheel–Rail Relationship

Xuesong Jin

State Key Laboratory of Traction Power, Southwest Jiaotong University, Chengdu 610031, China; xsjin@swjtu.cn

Abstract: The research on wheel–rail relationship includes the basic theoretical models and corresponding numerical methods of wheel–rail in rolling contact, geometric parameter matching and material matching of them, friction and wear, wheel–rail rolling contact fatigue, wheel–rail adhesion and noise. They are also key theoretical and technical problems of the high-speed train/track coupling system. The basic theoretical models of wheel–rail in rolling contact and the corresponding numerical methods are the basis and one of the basic means for solving other wheel–rail relationship problems. The other is the experimental means. Moreover, the modeling and analysis of coupling behavior of the train and track can only be realized by means of the wheel–rail rolling contact mechanics model and its corresponding numerical method. This paper mainly discusses some research work and achievements on high-speed wheel–rail relationship problems since China opened a high-speed railway system on a large scale. The discussions in this paper include the classic wheel–rail rolling contact theoretical models (analytical forms) and the modern wheel–rail rolling contact theories (numerical methods), their advantages and disadvantages, their application and future development direction of them. The reviewed research progress on the other wheel–rail relationships mainly expounds the thorny problems of the wheel–rail relationship encountered in the operation of China's high-speed railway, how to adopt new theoretical analysis methods, test means and take effective measures to solve these problems. It also includes research results of similar important reference values performed by international peer experts in related fields. Challenging and unsolved problems in high-speed wheel–rail relationship research are also reviewed in the full text.

Keywords: high-speed train/track; wheel/rail; rolling contact mechanics model; wheel–rail profile matching; wheel–rail material matching; friction and wear; rolling contact fatigue; wheel–rail adhesion; wheel–rail noise

Citation: Jin, X. Research Progress of High-Speed Wheel–Rail Relationship. *Lubricants* **2022**, *10*, 248. https://doi.org/10.3390/lubricants10100248

Received: 15 August 2022
Accepted: 18 September 2022
Published: 30 September 2022

1. Introduction

In October 1964, Japan built the world's first high-speed railway, the Tokai Shinkansen, with an operating speed of 210–230 km/h. In decades of its operation, this high-speed commercial operation line has attracted 90% of the passengers from Tokyo to Osaka. The train's operating time error is less than 1 min, and its energy consumption is 1/5 of that of automobiles, with no exhaust emissions [1]. Therefore, high-speed railway transportation has attracted great attention from all countries in the world. At present, many countries and regions around the world operate or are building high-speed railways. At present, the total length of high-speed railways in the world has exceeded 50,000 km, and the length of high-speed railways in China is about four-fifths of the world's total. The maximum commercial operation speed reaches 350 km/h, and the field test speed is about 500 km/h.

Because the train runs at a high speed for a long time, the additional impact load and its frequencies are high, the service environment of train and track structure materials will change and various hidden problems will gradually be exposed, which will threaten the operation safety. The driving, braking and normal operation of the train depends on the wheel–rail in rolling contact at high speed. Wheel–rail rolling contact behavior has a direct impact on train operation quality, running safety and transportation cost. The dynamical behavior of wheelset rolling on track is very complicated. A wheelset rolls

on a track at high speed, with the vertical, lateral and vertical translation of its center of mass, and rolling and yaw motions [2]. In driving or braking of the train, the wheelset may simultaneously roll and slip relative to the track. Such sliding may be slight or large [3]. Due to the wheel/rail contact geometry constraint and their movement characteristics, in their running, relatively small sliding in three directions always occurs between the contact surfaces of the wheel and rail (called the lateral, longitudinal and spin creepages) [3]. If the high-frequency flexible deformation and the local elastoplastic deformation of the wheelset and rail are neglected in the normal rolling contact state, the wheel/rail creepages can be expressed by a complete mathematical formula. They are determined by wheel/rail contact geometric parameters and wheelset motion parameters [3,4]. It is very difficult to accurately calculate the creepages while considering the effect of high-frequency flexible deformation and local elastoplastic deformation of the wheelset on them [5,6]. The creepages are the key parameters to characterize the relative motion of wheel–rail contact surfaces. They are the independent variables of the wheel–rail rolling contact model. The dependent variables of the model are called the creep forces between wheel/rail. So far, the dynamic simulation of the high-speed train system neglected the influence of high-frequency deformation of the wheel–rail structure and local elastoplastic deformation at the wheel–rail contact point in the calculation of the creepages [7,8]. However, their influence on the mechanism of high-speed wheel polygon wear and rail corrugation, adhesion characteristics, damage mechanisms of wheel–rail contact surface and wheel–rail noise generation mechanisms should be not ignored at high speeds [9,10].

The actual existence of wheel–rail rolling contact surface irregularities includes normal random roughness, period irregularity surface, wheel flat and rail scratch, rail welding joint, etc. The separation and impact of wheel/rail in rolling contact occur frequently [11,12]. This situation will accelerate the fatigue and injury of wheel/rail [13] and cause large impact noise [14]. It can also reduce the wheel/rail adhesion level and affect the normal traction and braking of the train [15]. The serious cases can lead to train derailment. In order to understand and solve these problems clearly, it is necessary to develop a more perfect theoretical model of wheel–rail in rolling contact to correctly characterize and assess their effects on the normal and safe operation of trains, even if containment and prevention measures are taken.

From the history and experience of high-speed railway operation around the world, the high-speed wheel–rail relationship is a very important and complex scientific subject. According to the basic function of wheel–rail rolling contact pair and the occurred problems in the process of their operation, the research on the high-speed wheel/rail relationship is divided into the basic theory of wheel/rail rolling contact, matching and optimization of wheel/rail profiles and materials, wheel/rail adhesion characteristics, contact surface wear, rolling contact fatigue and wheel/rail noise. Their research involves many subjects, such as tribology, system dynamics, solid mechanics, elastoplastic mechanics, fracture mechanics, material science, structural sound theory, etc. This paper reviews and summarizes the research work on the above problems of the wheel–rail relationship since China started running high-speed railways [16]. It also includes research results of similar important reference values performed by international peer experts in related fields. Challenging and unsolved problems in high-speed wheel–rail relationship research are also put forward in place in the paper.

2. Basic Theory of Wheel/Rail Rolling Contact

The basic theories of wheel–rail rolling contact mainly include the classical theoretical models of wheel–rail in rolling contact and the numerical theories and numerical methods developed in modern times. There are five classical theoretical models which reflect the relation between the total force components and the creepage components between wheel and rail in rolling contact state. The first is the one-dimensional rolling contact model of wheel–rail published by F. W. Carter in 1926, which describes the nonlinear relation law between the longitudinal creepage and the longitudinal creep force in the direction

of wheel–rail rolling [17]. The model is suitable for wheel/rail contact surfaces with such severe wear, which causes the wheel–rail contact patch to become elongated laterally, as shown in Figure 1. Figure 1a indicates that the new wheel and the new rail contact, forming an elliptical contact spot. After long-term operation, the wheel–rail contact surface is seriously worn, and the contact spot formed becomes lateral slender strips, as shown in Figure 1b. The model is still used in evaluating adhesion and traction between the locomotive wheel and rail [18]. The important theoretical contribution of F. W. Carter's model is that it adopted the two hypotheses, one being that the sliding of the wheel–rail contact surfaces starts from the rear edge of the contact patch and gradually expands to the front edge of the contact patch with the increase in the longitudinal creepage. Figure 2 shows the division of the slip–slip area of the wheel–rail rectangular contact patch, first established by Carter. The rectangular contact patch approximates the laterally elongated contact patch in Figure 1b. This hypothesis was verified to be correct using some numerical methods later [3,19]. The other contribution of the model is that the longitudinal width ratio of the adhesive zone to the whole contact area is a function of the ratio of the longitudinal creep force to the maximum total friction force in the contact patch, which is a mathematical analytic expression, as indicated by Equation (2). In Equation (2), a and a_s are the semi-axial lengths of longitudinal width of the contact patch and the adhesion zone, respectively, P_x is the longitudinal creep force of the wheel/rail, P_0 is the total normal load and f is the friction coefficient at the wheel–rail interface. The two hypotheses of this model were adopted in subsequent studies on the wheel–rail rolling contact models based on Hertz theory [3].

$$\frac{a_s}{a} = \left(1 - \frac{P_x}{fP_o}\right)^{\frac{1}{2}} \quad (1)$$

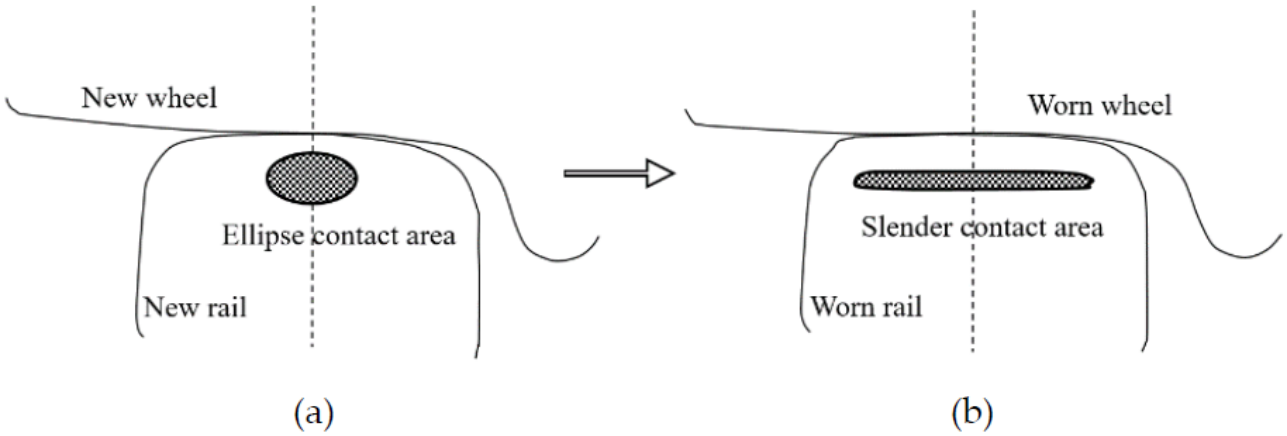

Figure 1. (**a**) New wheel and the new rail contact forming an elliptical contact spot, and (**b**) seriously worn wheel/rail contact forming a lateral slender contact area.

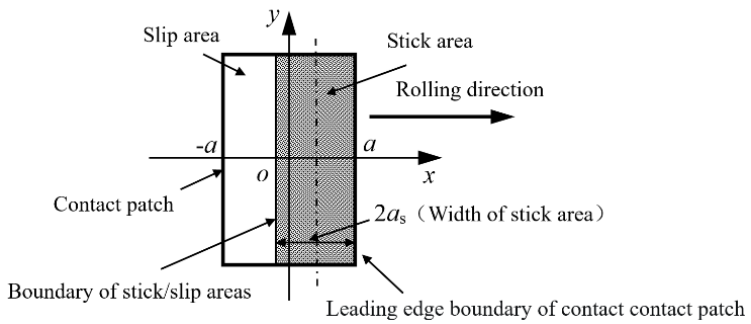

Figure 2. Division of the slip–slip area of the wheel–rail rectangular contact patch, first established by Carter.

Vermeulen and Johnson developed a model of wheel–rail in rolling contact based on Carter's research ideas. Their model is the mathematical analytical formula expressing the nonlinear relation between longitudinal/lateral creepages and forces. This model ignores the influence of wheel–rail spin creepage [20]. The relative rotation between wheel–rail interface is caused by the projection of the rolling angular velocity of the wheelset, Ω, onto the normal direction at wheel/rail contact points, as indicated in Figure 3. In the Figure, $\mathbf{N}_R$ is the normal direction at the right wheel/rail contact point. The direction of Ω always coincides with the axis of the wheelset. It is at angles of $(90 + \delta_R - \phi)$ and $(90 + \delta_L + \phi)$ with the common normal directions at the right and left wheel/rail contact points, respectively. δ_L and δ_R are, respectively, the left and right wheel/rail contact angles, and ϕ is the rolling angle of the wheelset. The projections of Ω onto the normal directions rely on them. The ratios of the projection to wheelset running speed, v_0, is defined as the wheel–rail spin creepage. The spin creepage has great influence on the amplitudes of longitudinal and lateral creep forces of wheel–rail and their density distribution direction [3]. The shapes of the wheel–rail contact patch and stick zone in it considered in this theoretical model are ellipsoids, as indicated by Figure 4.

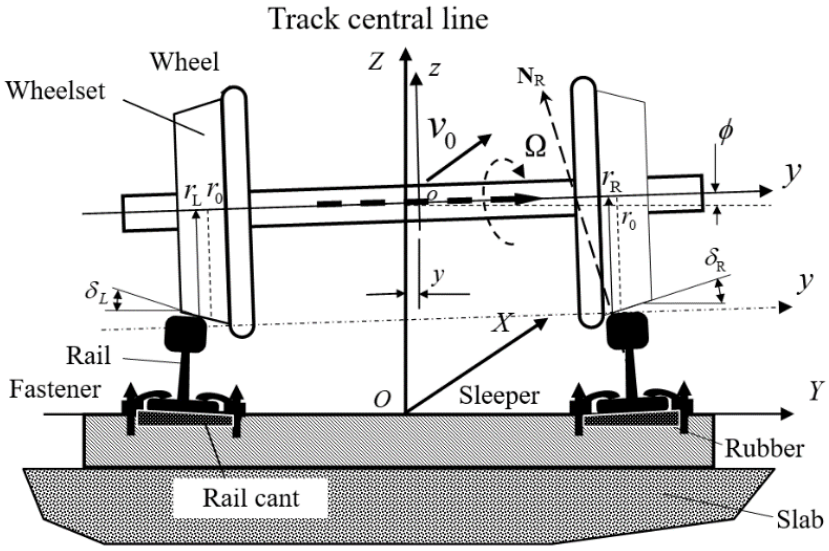

Figure 3. A schematic illustration of a wheelset rolling on a track.

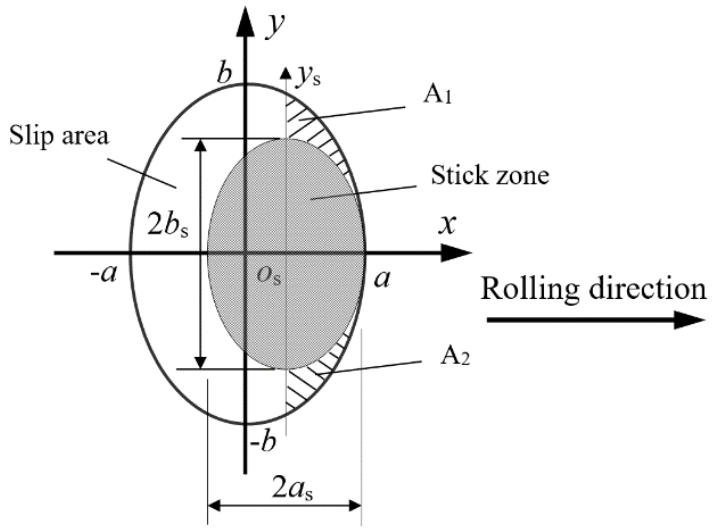

Figure 4. Division of stick–slip area in wheel/rail contact patch by Vermeulen and Johnson.

It is not correct to treat the two local areas symmetrical in the direction of rolling as sliding areas [3]. The areas are denoted by A_1 and A_2 in Figure 4. They are next to the leading edge of the elliptical contact patch. Especially for trains running on a tangent track, the model can effectively consider the lateral and longitudinal coupling of the wheel–rail system and carry out the rapid dynamic behavior simulation of large vehicle-track coupling system. However, when a train runs on a curved track, the outer wheel rim will contact the inner corner of the outer rail and in this case, the wheel–rail contact angle is large. The larger the wheel–rail contact angle, the greater the spin creepage between the wheel and rail, the greater the influence on the longitudinal and lateral creep forces of the wheel and rail and the greater the error of the dynamics simulation results [3]. This is because the model does not consider the influence of wheel/rail spin creepage on the wheel/rail creep forces.

In 1967, J.J. Kalker developed a linear wheel–rail creep theoretical model considering the effect of small spin creepage by means of series theory in his doctoral thesis, which established the linear relation laws of longitudinal and lateral creepages/creep forces, spin creepages/spin-moments of the wheel/rail [21]. Because Kalker could not introduce Coulomb's Friction Limitation Law when deducing the theoretical model, his linear creep-force theory reflects that wheel–rail creep-force increase can be unrestricted with the increase in wheel–rail creepage, which does not conform to Coulomb's Friction Law. It should be noted that it is only suitable for small creepage cases when applied [3].

By means of Vermeulen–Johnson's model and Kalker's linear model, Z.Y. Shen et al. developed a three-dimensional nonlinear wheel–rail creepage/creep-force model, considering the influence of the small spin creepage [22]. It is emphasized that the model is suitable for wheel–rail rolling contact with the small spin creepage, that is, the case of a small wheel–rail contact angle. This requirement indicates that there may be a certain error in analyzing wheel–rail rolling contact behavior by using this model when a train is running on sharp curved tracks. This is because the wheel flange contacts the inner corner of the outer rail.

The fifth classic wheel–rail creep theoretical model is called the simplified theoretical model (hereinafter, referred to as FASTSIM) developed by J.J. Kalker. It was developed with the help of the linear model of Kalker [23]. In this model it is assumed that the normal force distribution in the wheel/rail contact patch is in harmony with the clearance between the wheel/rail at contact point. The clearance is a mathematical expression for a quadratic paraboloid. The normal pressure distribution in the contact patch is no longer an ellipsoid distribution form, but a quadratic parabolic distribution form. This is different from the wheel/rail normal pressure distribution considered in the establishment of the four classical Hertzian creepage/creep-force models discussed above. In the FASTSIM, it is assumed that the three surface force components in the contact patch have a linear relationship with the corresponding three displacement components in the contact patch and the coupling effect of them is ignored. This model can be used to calculate not only the creep forces of the wheel/rail, but also the distribution of the slip and tangential forces in the elliptical contact patch. However, the calculation speed is lower than that of the previous four theoretical models.

It is worth noting that establishing the above five theoretical models relies on the Hertz contact theory hypothesis, so they are called the Hertzian calculation models. These models do not include the influence of wheelset running speed explicitly, although the creepage is defined as the ratio of the speed difference at the wheel–rail contact interface to wheelset speed. However, at present, the dynamic behavior simulation of the large vehicle-track coupling system still relies on the models discussed above, regardless of train operating speeds. The Hertz contact theory hypothesis includes that the contacting surfaces of two bodies in contact are smooth, their material is within elastic range and the radius of curvature at or near the contact point is much larger than the characteristic radii of the contact patch. It is difficult to strictly meet the Hertz theory hypothesis in the actual operation state of wheel and rail. The neglected factors (such as the normal and

abnormal irregularities of wheel–rail contact surfaces, the actual geometries of wheel/rail, plastic deformation, etc.) may have an influence on the coupling dynamic behavior of the vehicle-track system to a certain extent. However, their influence on the local behavior of wheel/rail (such as wear, elastoplastic deformation, rolling contact fatigue, adhesion and wheel/rail noise) cannot be ignored, especially in severe cases, such as rail corrugation, wheel polygonal wear, rail welded joints, wheel/rail scratch, contact surface flaking, etc. It is impossible to analyze the effects of these factors by using these models [24–27]. It is necessary to develop more advanced wheel–rail rolling contact models and corresponding numerical methods to consider the influence of the above factors on wheel–rail rolling contact behavior.

Modern wheel–rail rolling contact theories and corresponding numerical methods are developing. In the 1970s, J.J. Kalker expressed the rolling contact problem of two elastic bodies with friction by using the variational inequality according to the variational principle. The solution of the rolling contact problem was determined by solving the force density components on the contact patch, satisfying the minimum residual energy principle of two elastic contact bodies [28]. The corresponding numerical program is called CONTACT, which has been widely used by railways around the world to analyze wheel–rail rolling contact behavior. This theoretical model breaks through the assumptions of Hertz contact theory. So, it is called the Non-Hertz rolling contact theory model. The program can be used to calculate the relevant information of wheel/rail in rolling contact, some of which cannot be calculated by the above five classical wheel/rail rolling contact theoretical models. For example, the true shape of the wheel/rail contact patch after wear, stick–slip areas in the contact patch, the amplitude and direction distribution of tangential force components, normal pressure, distributed slip and stress field in wheel/rail body, etc. [3]. They are useful in the analysis of wheel–rail fatigue and rolling contact noise. However, compared with the classical creep-force models above, its calculation speed is much slower. It is not suitable for fast simulation analysis of dynamic behavior of the large-scaled vehicle-track coupling system. Its numerical realization process is based on the theory of elasticity in half-space, and the numerical results of wheel–rail normal force are slightly larger than those of the current finite element model [29,30]. This is because wheel and rail are regarded as elastic half-space objects, which actually exaggerates the contact stiffness of wheel–rail. The influence of wheel–rail contact on plastic deformation should not be neglected [30].

X.S. Jin et al. made a detailed analysis and comparison of the numerical analysis results of wheel/rail in rolling contact by using the five above calculation models (Carter's model not included). In the analysis, the wheel–rail motion states considered are general and representative. The numerical results showed that, except for Kalker's linear theoretical model, the approximation degree of the results of the other models is acceptable [3]. Considering the need for rapid numerical simulation of the vehicle-track coupling dynamics, especially for high-speed train or vehicle-track coupling dynamics, the wheel–rail creepage/creep-force model proposed by Z.Y. Shen et al. not only considers the influencing of the longitudinal, lateral and spin creepages, but also has high computational efficiency, because it is an analytical expression. Even in the case of wheel rim in contact with rail gauge corner, that is, for the large wheel/rail contact angle or the large spin creepage, there is little difference between the calculation results of Shen's model and CONTACT. Later, X.S. Jin et al. further improved Kalker's CONTACT model by using the finite element method [3,31,32], and the improved model could take into account the influence of the outer boundary conditions of the wheel–rail contact point on wheel/rail rolling contact behavior. However, it is a pity that the theoretical model has not realized numerical calculation.

By means of the parametric variational principle quadratic programming method and finite element method, the calculation method developed by W.X. Zhong and H.W. Zhang can be used to analyze the wheel–rail elasto-plastic contact problem [33]. The parametric variational principle is more widely used than the classical variational principle. It can avoid the Drucker hypothesis used in material plasticity theory and effectively deal with the problem of irreversible flow of elasto-plastic materials and friction contact with

sliding. This method was successfully used to analyze wheel–rail elastoplastic rolling contact behavior in transient braking and driving of a wheel rolling on a rail [34].

Since the 1980s, the finite element method has been used to analyze wheel–rail rolling contact behavior. In the early stages, the wheel–rail contact finite element model is relatively simple [35,36]. Oden and Lin proposed an analytical expression to represent a two-dimensional rolling contact problem. Later, the two-dimensional analytical solution was extended to the three-dimensional case [37,38]. Nachenhorst Udo introduced stick–slip contact control conditions in his doctoral thesis [39], the fluid layout gradient decomposition method and the Arbitrary Lagrange–Euler Method were used to analyze the rolling contact behavior of 3D elastic bodies, and the fine mesh adaptive technique was used in the analysis. His numerical method was used to solve the steady rolling contact problem of three-dimensional elastic bodies. The considered rolling speed is low (10 km/h), and the contact surfaces are smooth without sliding between them [40].

In the service process of wheel–rail, the wheel and rail experiences repeated acceleration and deceleration, wheel/rail running surfaces exhibiting various defects, such as cracks, surface material stripping and uneven wear. The wheel–rail rolling contact process is a transient elastoplastic rolling contact behavior with the operation speed changing. Namely, the rolling contact behavior varies with the operation speed and time. In these cases, the rolling contact theories discussed above cannot be used to clearly explain the wheel–rail rolling contact behavior and corresponding mechanism problems. The wheel/rail rolling contact model established based on the finite element method can consider more factors discussed above.

With the help of commercial software ANSYS/LS-DYNA, X. Zhao and Z.L. Li developed a three-dimensional elasto-plastic model of wheel–rail in rolling contact [29,30], and analyzed the wheel–rail impact behavior caused by rail squat [41]. In their model, the actual geometric dimensions of wheel and rail, the unsprung mass of the vehicle and the parameter characteristics of the track are taken into account. The wheel rolling speed is 40–140 km/h, and the wheel–rail contact boundary model adopts the face-to-face contact element method. Based on their model, a high-speed wheel–rail 3D elastoplastic finite element model was developed, as shown in Figure 5. This model also takes into account the actual dimensions of the track (rails, fasteners, sleepers and track plates, as well as mortar lay and the sprung mass of the wheel) [30,42].

The model is used to analyze the influence of many factors on high-speed wheel–rail rolling contact behavior successfully and effectively. These factors include rail corrugation, crack, wheel polygon wear, scratch, material inclusion, high speed, etc. The numerical results with important reference values are obtained. These results can effectively help us to clarify the evolution process and causes of the concerned wheel/rail damage state in high-speed operations. It provides important guidance for improving wheel/rail material, wheel/rail production technology and wheel/rail maintenance strategy and ensuring safe operation of trains at high speeds.

Since the operation of the high-speed railway in China, rail corrugation occurred in some rail lines [16], as shown in Figure 6. The additional dynamic loads caused by rail corrugation with different wavelengths, depths and operating speeds need to be further understood. They are the basis for evaluating high-speed safe operation, key component fatigue life assessment and maintenance strategy formulation. However, the current instrumented wheelset for measuring dynamic wheel–rail loads cannot accurately measure high-frequency additional dynamic loads between the wheel and rail (500–1100 Hz [16]) under the excitation of rail corrugation. A numerical method is still the only way to calculate the actual dynamic load between the wheel and rail in a high-frequency range.

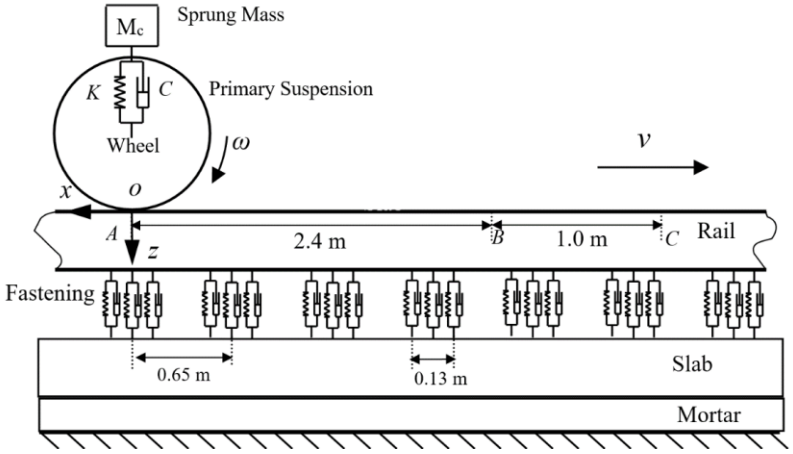

(**a**) Schematic diagram of wheel/rail rolling contact calculation model

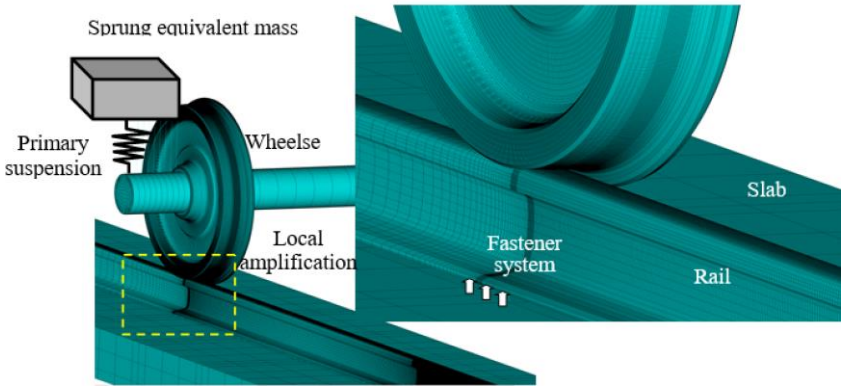

(**b**) Wheel–rail finite element mesh

Figure 5. Three-dimensional elasto-plastic finite element calculation model of wheel–rail in rolling contact.

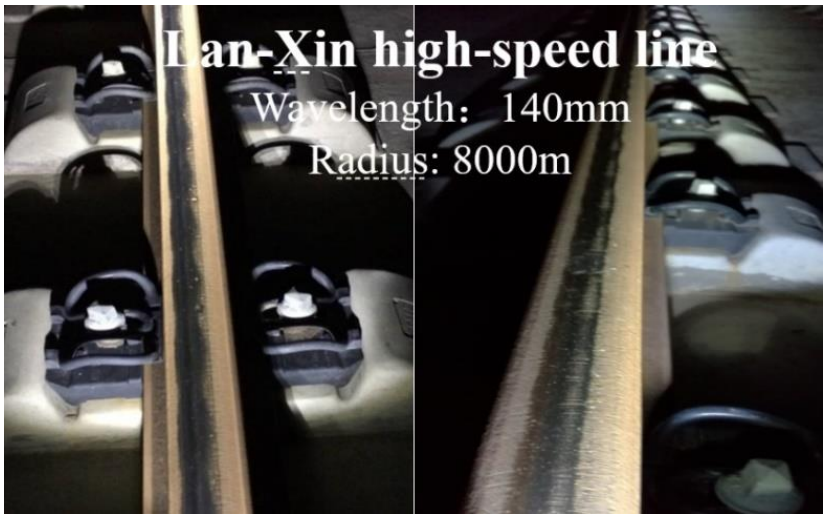

Figure 6. Rail corrugation photos of high-speed line.

Figure 7 shows the maximum and minimum values of the wheel/rail vertical dynamic load at an operating speed of 300 km/h which varies as the depth of rail corrugation with 60mm wavelength increases. The black lines in Figure 7 represent the calculation results, obtained by using a traditional vehicle-track coupling system dynamics model. The red lines represent the results of the current three-dimensional finite element model of wheel–

rail. Obviously, the calculation results of the two models are different. The amplitudes of fluctuation of the additional dynamical load, calculated by using the traditional dynamic model, are much larger than those calculated by the elasto-plastic finite element model. This is because in the wheel–rail normal direction, the traditional dynamics model uses the Hertz contact model to couple the vehicle subsystem with the track subsystem [43]. The calculation results of it show that the wheel/rail vertical dynamic load is exaggerated. The reason is that the elastic half-space hypothesis in Hertz contact theory overstates the actual wheel/rail contact stiffness [3].

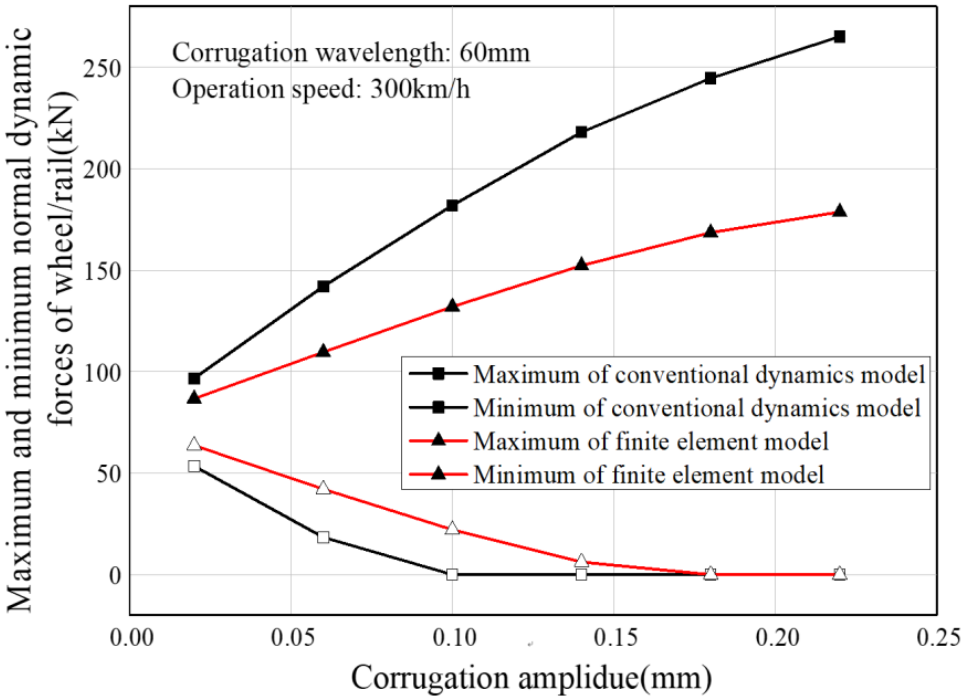

Figure 7. Comparison of wheel/rail vertical dynamic loads calculated by the two models.

Another important phenomenon, as seen in Figure 7, is the case where some of the minimum wheel–rail dynamic loads are zero, which indicates that the wheel has separated from the rail. Too long of a wheel–rail separation time in high-speed operation will pose a threat to safe running. The length of separation time is strictly limited [43]. The additional dynamic load difference calculated by the two models has a great influence on the evaluation of the operation safety index, the service life of the concerned components and developing the maintenance strategy of wheel and rail. It is worth further discussion.

A successful example of rolling contact behavior under wheel/rail damage condition was calculated by using the current finite element model. Figure 8 shows a calculation model of a wheel that rolls over a vertical crack of rail head at 300 km/h. The model takes into account half a wheelset, sprung mass and half an actual track. The right figure in Figure 8 indicates the distribution of the grid nodes of the finite element mesh near the vertical crack. Figure 9a shows that the tangential force density distribution at the wheel–rail interface was calculated at different points in time by using the current high-speed 3D wheel–rail elasto-plastic model. Figure 9b denotes the friction distribution on the crack surface during wheel rolling over the crack [44]. It is obvious that the information shown in Figures 7 and 9 cannot be calculated by using the classical wheel–rail rolling contact theory models. The information is very useful for accurately evaluating the wear of wheel–rail contact surfaces with cracks and crack propagation.

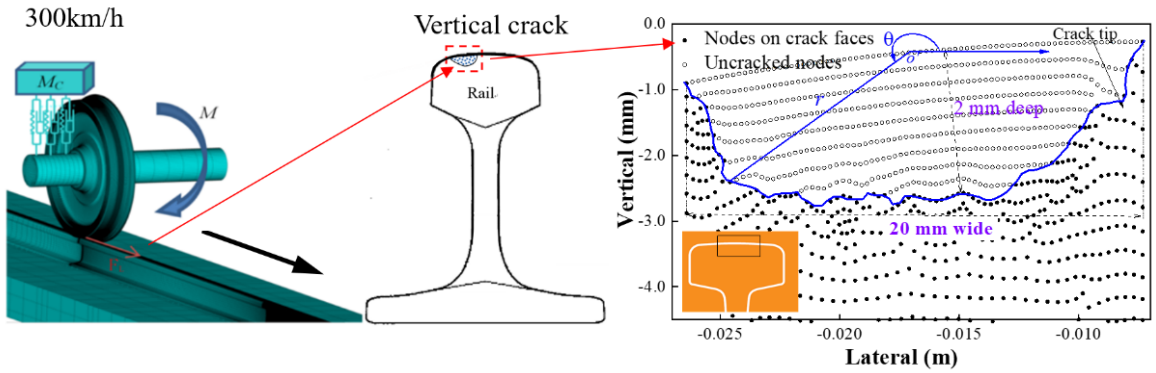

Figure 8. Wheelset rolling over a rail with a vertical crack in the rail head.

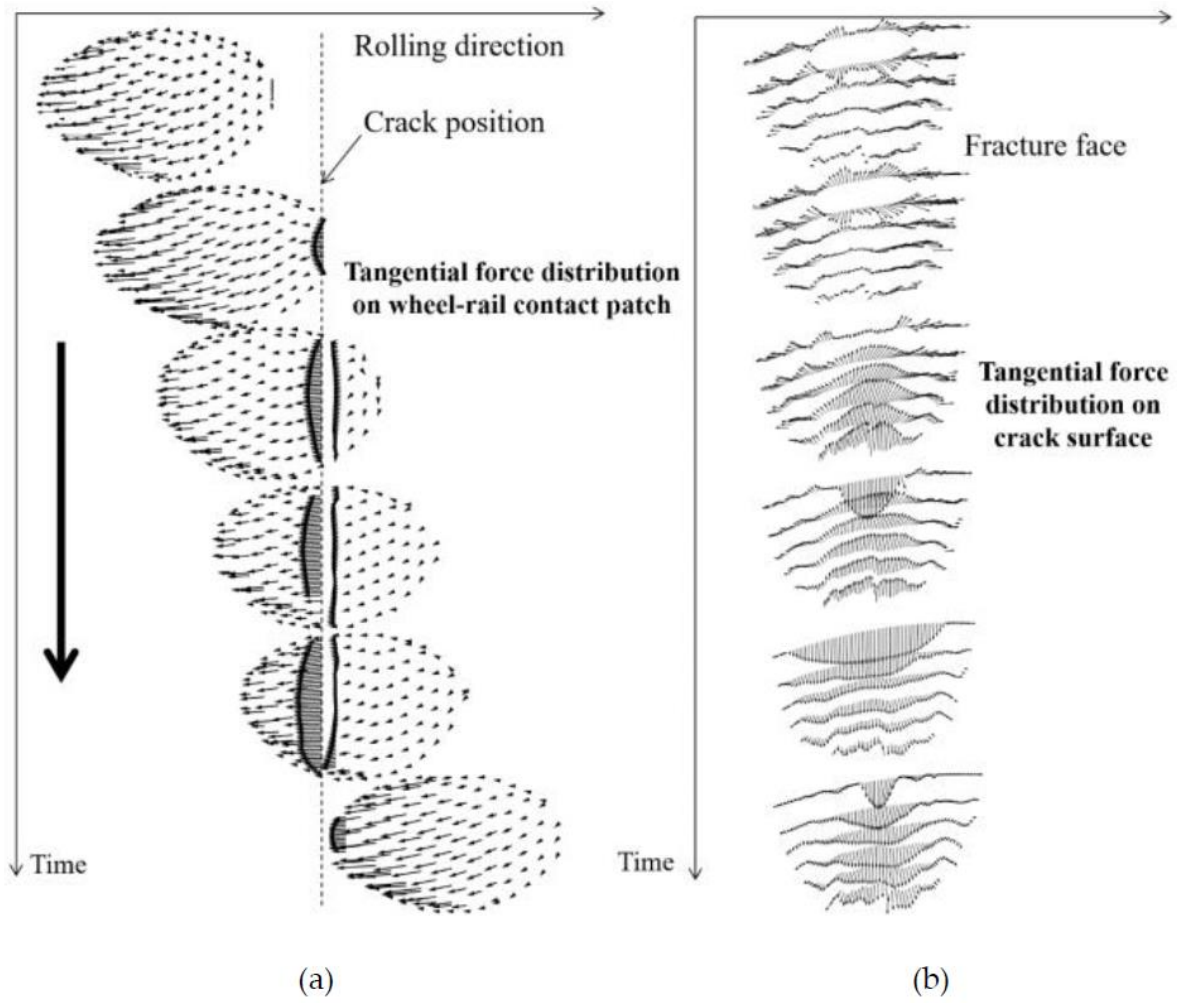

Figure 9. (**a**) Tangential force density distribution in wheel–rail patch during wheel rolling over a vertical crack; (**b**) friction distribution on crack surface of rail.

The current 3D elastoplastic rolling contact model still cannot consider the influence of the wheel–rail interface state (micro-roughness, the third medium (water film, sand and pollutants) and the environment (temperature, humidity, etc.)) so far. These problems will be discussed below.

Wheel–rail running causes wheel polygonal wear, rail corrugation and noise. These are related to the high-frequency vibration of wheel–rail structure and their motion characteristics [45–48]. Many scholars considered the influence of high-frequency flexibility of the wheelset in the vehicle-track coupling dynamics models [49–54]. In these stud-

ies, the influences of wheel–rail flexible deformation on wheel–rail rolling contact behavior and the contact geometric calculation were not discussed in detail. It is also a complex research problem.

The doctoral thesis of S.Q. Zhong carefully discussed the influence of wheelset deformation characteristics and its high-speed rotation on wheel–rail rolling contact behavior and vehicle-track coupling behavior. The research content of the dissertation is divided into three parts [55]. Firstly, the influence of the first several order bending of wheelset axle was analyzed, as shown in Figure 10 [6]. The wheelset axle was modeled as a Euler–Bernoulli beam, and the left and right wheels were modeled as rigid bodies fixed to the axle. Based on the Euler–Bernoulli beam bending vibration theory, the axle-bending vibration equations were established in the two planes. One plane is parallel to the track plane, and the other is perpendicular to the plane of the track and on the centerline of the track. At the same time, a geometric calculation model of wheel–rail contact was established, considering the influence of the wheelset axle deformation. It was assumed that the cross-sections of the two wheels did not deform and their rolling circles were always perpendicular to the axle line at the centers of the rolling circles after the wheelset axle was deformed. Modal superposition method was used to solve the wheelset dynamics equations. Please refer to Reference 6 for the symbolic meaning in Figure 10. Figure 11 shows the comparison of the wheel/rail dynamical vertical forces. They were calculated by the two vehicle-track coupling dynamics models at the operation speeds from 200 km/h to 400 km/h. The wheelset axle deformation considered the first three bending modes, and their corresponding modal frequencies are 117 Hz, 203 Hz and 350 Hz, respectively. It was considered that the harmonic excitation with a wavelength of 0.2378 m and an amplitude of 0.01 m represents the excitation of existing rail corrugation. The first three bending modes were excited, corresponding to the three peak values of the wheel/rail vertical force (f_{m1}, f_{m2} and f_{m3}), as shown in Figure 11b. The peak denoted by f_{ir3} represents the response to the harmonic excitation. It should be noted that the bending vibration of the wheelset is easy to cause the polygonal wear of the wheel under certain conditions [9,10].

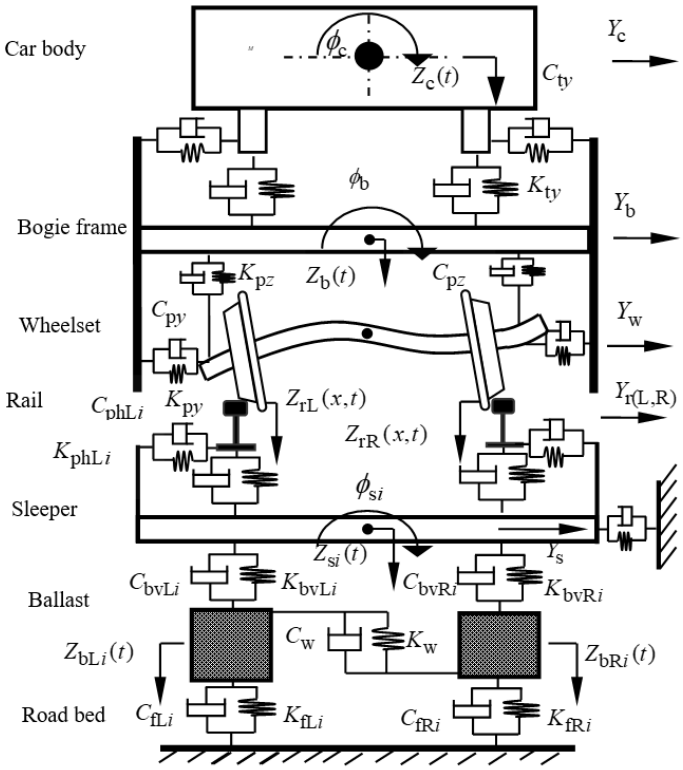

Figure 10. Vehicle-track coupling model with considering effect of the deformed wheelset axle.

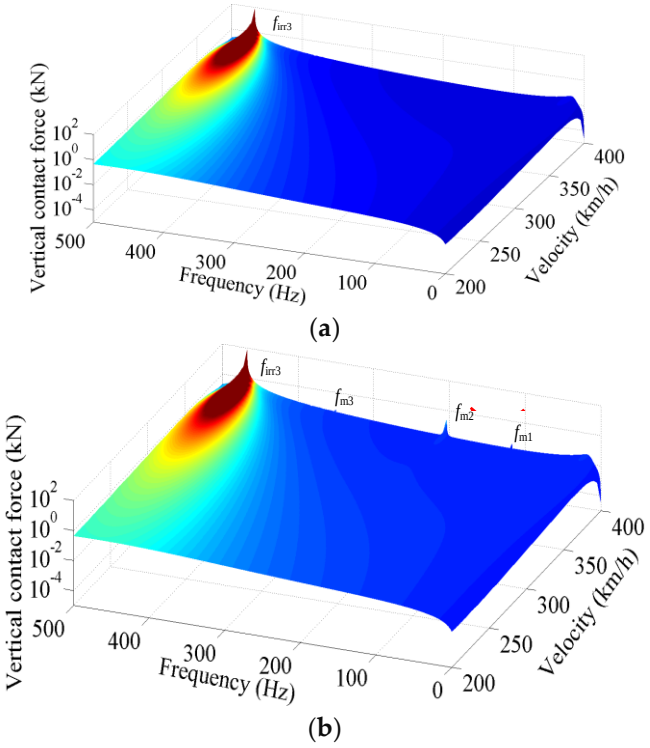

Figure 11. Comparison of wheel/rail vertical forces calculated by two vehicle-track coupling dynamics models (**a**) without wheelset deformation; (**b**) with wheelset deformation.

Secondly, the finite element method was used to establish a new model of a flexible wheelset. It considers the higher frequency flexible deformation, such as the umbrella modes and nodal-diameter modes of the wheel, as shown in Figure 12. Figure 12a,b indicate the first unsymmetrical umbrella mode and the three nodal-diameter mode, respectively. At this point, the above wheel–rail contact geometry calculation model needs to be further developed in order to consider the influence of the umbrella modes on the wheel–rail rolling contact. In order to simplify the complex geometry calculation of wheel–rail contact, the deformation of the wheel rim was ignored.

Figure 12. (**a**) Umbrella mode, 500 Hz; (**b**) 3 nodal-diameter mode, 1177 Hz.

It was assumed to be rigid because the cross-section deformation of the rim was very small. In improving the wheel–rail contact geometry calculation model, the dummies of two half-rigid wheelsets were introduced, as shown by Figure 13 [55,56], which was the key to solving the problem. It was assumed that the partial boundaries of the unchanged cross-sections of the wheel rims always coincide with those of the two wheel rims of the two dummies. It can be seen from the wheel profile represented by the blue dotted line in Figure 13. Thus, the spatial position of the wheel rims of the flexible wheelset was determined by using the two dummies. In Figure 13, the deformation of the two-point connecting lines on the rim section was very small and it was assumed that they were

rigid, as indicated by $\overline{B_{DR1}B_{DR2}}$, $\overline{B^1_{DR1}B^1_{DR2}}$ and $\overline{B^2_{DR1}B^2_{DR2}}$. Reference [55] gave the detailed description on the complex and tedious modeling, considering the effect of wheel umbrella modes on contact geometry calculation.

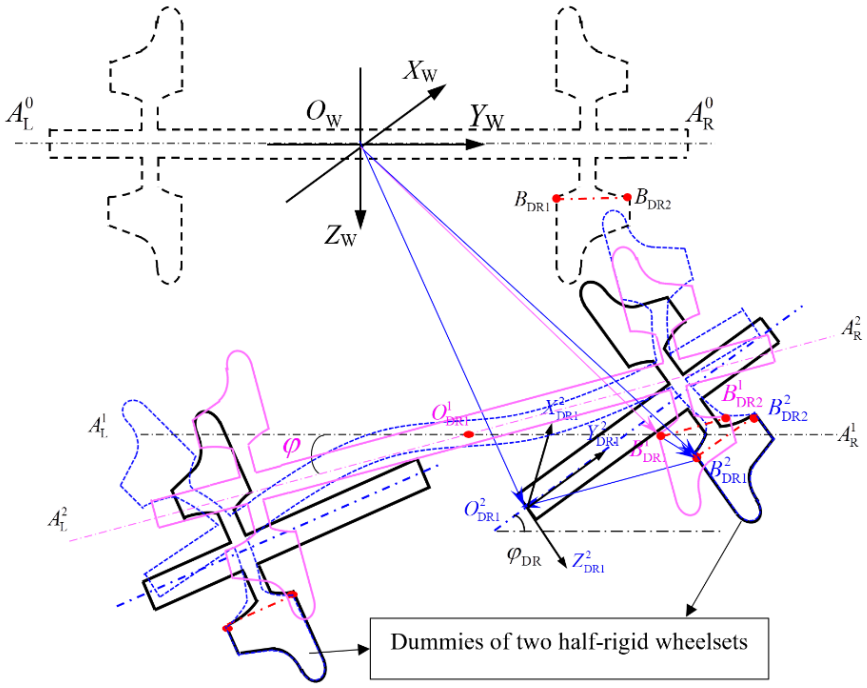

Figure 13. Relationship between the two rigid half-wheelset dummies and the flexible wheelset.

The wheel/rail normal force and wheelset sound pressure level, at 300 km/h and under the random vertical excitation from wheel–rail interface, were calculated by using the vehicle-track coupling dynamical model, considering the effect of the flexible wheelset model and the rigid wheelset, respectively. The frequency range of the random vertical excitation is 0 to 4800 Hz, and the amplitude is 0.02 mm. Figure 14 indicates the comparison of the wheel/rail normal forces of the two models. The influence of several high-frequency wheelset modes is highlighted, as shown by the peaks in the red curve. Figure 14 shows the four high-frequency modes of wheelsets, which correspond to the four prominent peaks of the red curve. The peak of f_s is the response to the discrete sleeper support excitation.

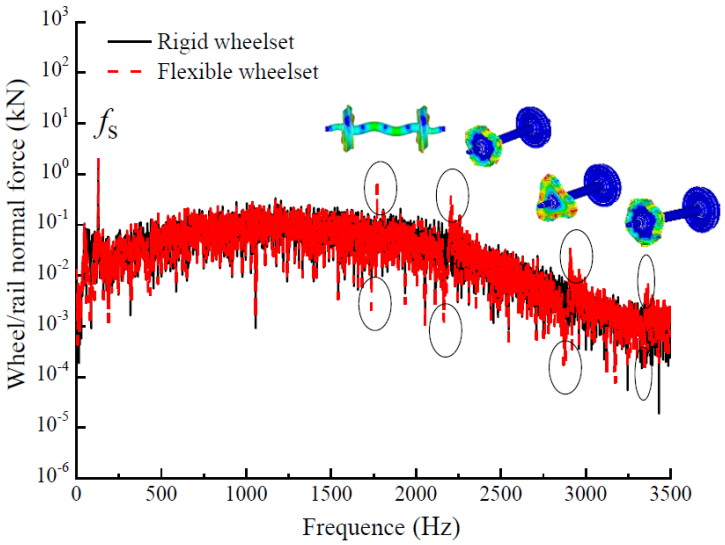

Figure 14. Wheel/rail normal forces in frequency domain.

Figure 15 denotes the sound pressure levels of the wheelset in frequency domain by using the two models. It is obvious that the several high-frequency wheelset deformations (or high-frequency modes), shown in Figure 14, have significant effects on the sound pressure level of the wheelset.

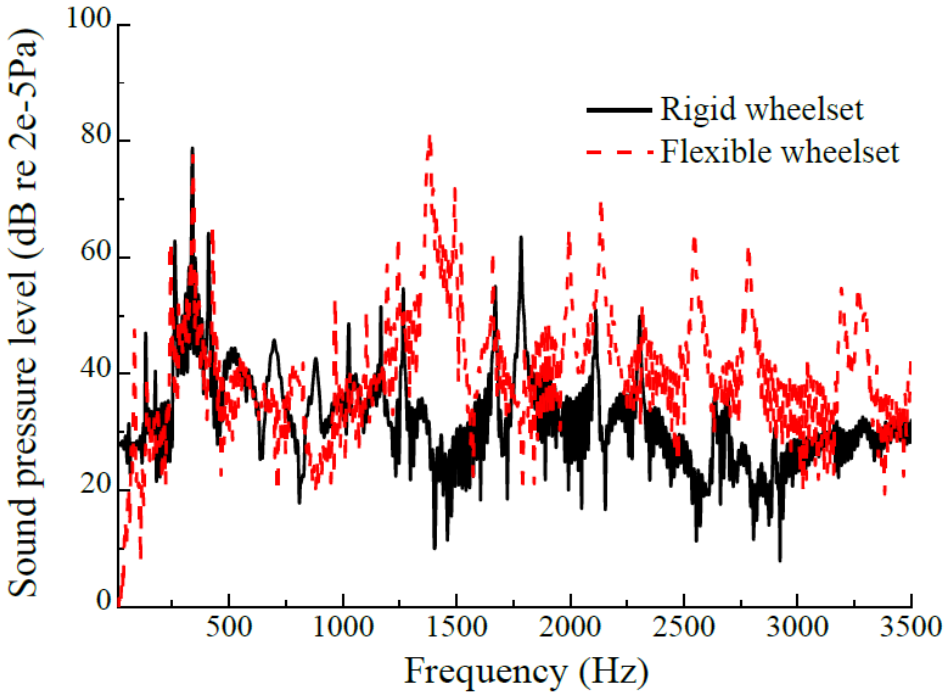

Figure 15. Sound pressure levels of the two models in frequency domain.

Finally, another new flexible wheelset dynamics model was established to consider the rotation effect of the wheelset. The motion equation of the wheelset, considering the rotation effect, is written as [55]:

$$\begin{aligned}&\ddot{\mathbf{q}}+2\rho\Omega\int_{Vol}\left(\sum_{i=1}^{3}\widetilde{u}_i\frac{\partial\mathbf{\Phi}^{\mathrm{T}}}{\partial u_i}\right)\mathbf{\Phi}dv\dot{\mathbf{q}}\\&+\left[\mathbf{K}-\rho\Omega^2\int_{Vol}\mathbf{\Phi}^{\mathrm{T}}\sum_{i=1}^{3}u_i\frac{\partial\mathbf{\Phi}}{\partial u_i}dv+\rho\Omega^2\int_{Vol}\mathbf{\Phi}^{\mathrm{T}}\left(\sum_{j=1}^{3}\sum_{i=1}^{3}\widetilde{u}_i\widetilde{u}_j\frac{\partial^2\mathbf{\Phi}}{\partial u_i\partial u_j}\right)dv\right]\mathbf{q}\\&=\mathbf{Q}+\rho\Omega^2\int_{Vol}\mathbf{u}^{\mathrm{T}}\mathbf{E}\mathbf{\Phi}dv\end{aligned}\tag{2}$$

where $\mathbf{\Phi}$ and $\mathbf{\Phi}^{\mathrm{T}}$ are, respectively, the modal matrix of the wheelset and its transpose matrix, $\mathbf{q}$ is the generalized coordinate column vector of the wheelset, $\dot{\mathbf{q}}$ and $\ddot{\mathbf{q}}$ are, respectively, the first and second derivatives of $\mathbf{q}$, $\mathbf{u}$ is the column vector matrix of the position of the wheelset at any point at the initial time, u_i and u_j ($i, j = 1, 2, 3$) are the components of $\mathbf{u}$, Ω is the rolling angular speed of the wheelset along the track, $\mathbf{K}$ is the stiffness matrix, $\mathbf{Q}$ is the generalized force matrix acting on the wheelset, ρ is the wheelset material density, $\widetilde{u}_i$ ($i = 1, 2, 3$) is the component of transfer matrix of $\mathbf{u}$ and $\mathbf{E}$ is a constant matrix of three times three, and in it $E_{11} = E_{33} = 1$ and the other elements are zero. An analytical transfer function of wheelset was also given in [55] and omitted here.

Figure 16 shows the frequency response functions of the flexible wheelset at speeds of 0 and 300 km/h, with and without considering the wheelset's rotation effect, respectively. Zero speed means that $\Omega = 0$ in Equation (2), namely the influence of the rotational angular speed of the wheelset is ignored. In Figure 16, the above figure represents the calculation result of 0–800 Hz, and the bottom figure is the result of 800–2400 Hz. $f_{\text{band-}i}$ ($i = 1, 2, \ldots, 7$) indicates the band frequency of the wheelset. Obviously, the rotational angular velocity makes the axle-bending frequencies bifurcate, and with the increase in the bending frequency, the frequency bifurcation of the wheelset-bending vibration tends to decrease.

$f_{(n,m)}$ indicates the frequency of nodal-diameter and pitch-circle modes. The foot symbols, n and m, represent the number of pitch-diameters and pitch-circles, respectively. Obviously, only $f_{(4,0)}$ is forked. $f_{um\text{-}i}$ (i = 1, 2, 3) denotes the frequency of the umbrella mode. Wheelset rotation has little effect on the wheel's umbrella mode frequency.

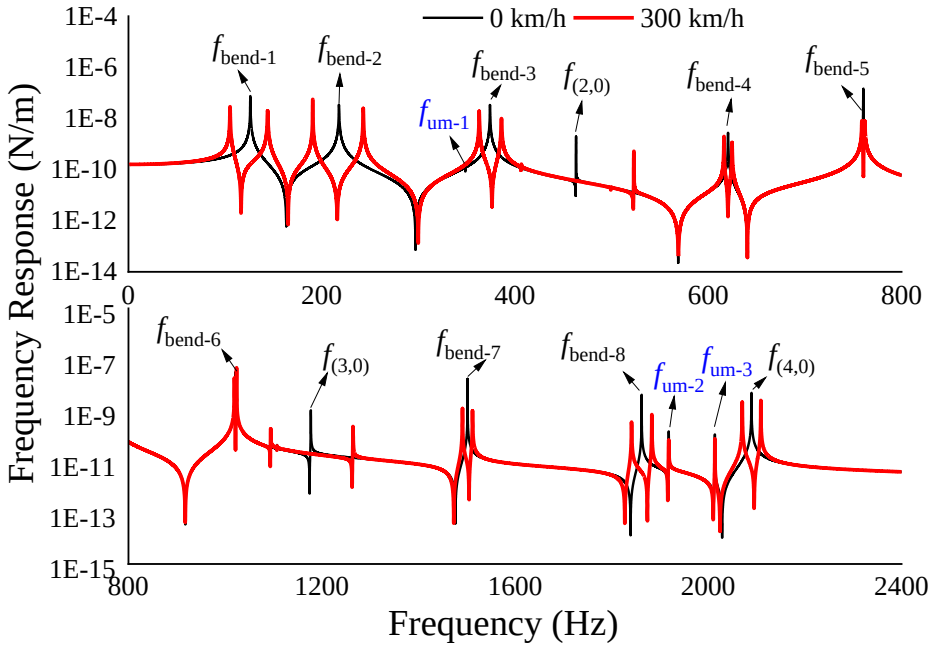

Figure 16. Frequency response functions of the flexible wheelset at 0 and 300 km/h.

J. Han et al. discussed the influence of wheelset rotational angular speed on wheel–rail rolling contact behavior and vehicle-track coupling dynamic behavior in the actual high-speed running [47]. The numerical results show that the influence of the rotational angular speed cannot be clearly identified. Its influence is completely submerged, compared with the influence of geometric eccentricity of wheel, random roughness excitation on wheel–rail contact surfaces, discrete sleeper support, etc. Therefore, in the future in-depth study of high-speed train-track coupling dynamic modeling, whether it is necessary to consider the influence of rotational angular speed of wheelset needs to be further discussed. Because of the influence of rotational angular speed of the flexible wheelset considered in the dynamic modeling of high-speed train-track coupling and the corresponding numerical analysis, the modeling becomes very complicated and the numerical calculation takes a lot of time.

For the actual wheel–rail rolling contact behavior, it cannot be described in details by the current theoretical and experimental methods. The process and mechanism of some problems induced by wheel–rail rolling–sliding contact behavior are still unclear. These problems mainly include wheel–rail adhesion characteristics, short pitch rail corrugation, wheel–rail rolling noise and squeal, interaction between rolling contact fatigue, wear and material properties of wheel and rail, etc. In addition, at present, the model of wheel–rail rolling contact only considers a single wheel and a single rail or half-wheelset and half-track structure with unsprung mass. Its scope of application is limited. Whether the train runs in a straight line or curve, strictly speaking, its dynamic behavior and structure are asymmetric with respect to the central vertical plane of the track. The dynamic behavior (including structure features) of the track, wheelset and vehicle are different along the train's direction of movement, but they influence each other. The rolling contact behavior of the wheel and rail at different positions of the same train is affected differently. That is to say, the development direction of the wheel–rail rolling contact model has two aspects. One is to consider the influence of a wheel–rail structure's microscopic factors and material nonlinearity, and the other is to consider the influence of the environmental structural features that constraint wheelsets and rails. Professor Z.L. Li's research team at Delft

University in the Netherlands has been active in this area in recent years. Yang and Li carried out an in-depth analysis on the characteristics of the waves in rail surface, induced by wheel/rail rolling contact [57]. These wave phenomena were produced by using the explicit finite element model of wheel–rail rolling contact, but they have not attracted much attention from relevant researchers. According to the mechanism of the rolling contact-induced waves, they divided these waves into impact-induced, creepage-induced and perturbation-induced waves. The relation between the generation of perturbation-induced waves and the stick–slip contact mechanism was discussed. The creepage-induced wave was proved to be a Rayleigh wave by analyzing the rail surface nodal motion forming the wave. Their research method and results also confirm that the explicit finite element model of wheel–rail rolling contact can effectively simulate physical rolling contact-induced waves and provide reliable dynamic contact solutions for wheel–rail. The effect of surface crack on the wave was studied by the finite element model, which provides a theoretical basis for crack detection based on the wave characteristics. The research ideas and results are of important reference value for the further study of the mechanisms of longitudinal vibration, short pitch rail corrugation, adhesion characteristics, squeal noise and surface crack of wheel/rail in rolling contact. Z. Yang et al. [58] systematically discussed the core algorithm of the explicit finite element method and theoretically proved that the explicit finite element method handles nonlinearities in friction, material properties, arbitrary contact geometries and boundary conditions, and fully couples the calculation of frictional rolling contact with the calculation of high-frequency structural dynamics. In order to promote the wide application of this method, detailed steps for establishing a robust wheel–rail dynamic interaction model and obtaining the dynamic contact response were presented. Shen et al. [59] used two models to analyze the differences in the time and frequency domain of the impact force of the wheel and rail caused by a typical rail squat. The beam model and the continuum model (finite element model) were, respectively, considered in the track modeling of the two models. It was found that the continuum model is more accurate than the beam model by comparing to field observations with the numerical results. In engineering practice, this study can assist engineers in choosing the appropriate assumptions for the wheel, contact and track models when solving wheel–rail impact problems. In the paper [60], a three-dimensional elasto-plastic finite element model of wheel–rail interaction was established to explore the possibility of martensite phase transition in wheel–rail materials under the influence of thermal energy caused by wheel–rail rolling friction for a critical creepage case.

The paper [61] puts forward a high-speed wheel–rail transient rolling contact model accounting for the nonlinear displacement-force properties of hanging sleepers. This model was used to analyze the impact contact behavior of wheel–rail caused by the sleeper suspension induced by the irregular rail geometry when the wheel passes over the suspension sleeper at a high speed. At the same time, it was found that the sleeper suspension defect has little effect on the stick–slip state distribution and rolling contact fatigue. The knowledge obtained can provide guidance for assessing the safety condition and maintenance of high-speed ballasted railway tracks.

3. Optimal Matching Design of High-Speed Wheel–Rail

Railway has developed for nearly 200 years, and train running speed has increased from about 10 km/h to 350 km/h. However, the wheel–rail matching problem has not been completely solved so far. The wheel–rail matching problem mainly includes two aspects: geometric size and profile matching, and material matching. Geometric size matching needs to consider the wheelset geometric sizes, track gauge and rail cant. Usually in the design and construction of railway vehicle and its track, these parameters are determined in advance. Then, according to the criteria, which are, respectively, minimum wheel–rail contact stress, minimum wheel–rail wear, excellent passing ability of wheelset on curved track and higher stable running speed on straight track, the profiles of the wheel and rail top are optimized to meet these criteria [62]. In practice, it is very hard to satisfy these

criteria at the same time. Due to the continuous progress of metallurgy and heat treatment technology in the past 20 years, the wear resistance of wheel/rail materials has been greatly enhanced. Therefore, the high-speed rail wear is quite light in the service process, except for rails of sharp curved tracks to train depots [63]. Moreover, high-speed wheel–rail rolling contact fatigue is not serious, compared with heavy-haul railway, urban railway and the existing railway with mixed passenger and freight transport at speeds less than 120 km/h. One of the most important reasons is that, in the high-speed operation section of high-speed lines, the radii of the curved tracks are large (generally more than 3000 m). When the train passes through the curved tracks of large radii at high speeds, the wheel rim is not easy to contact the inner corner of the high rail, and no serious wear occurs at the corner of the rail. At the same time, the wear of a high-speed train's wheel rim is also reduced. Therefore, the top profile of the rail in the high-speed operation line section is stable in long-time service. At high speeds, the stability of the train is very sensitive to the change in the wheel tread or the change in the wheelset conicity, due to wear. The optimization design of high-speed wheel profile is priority in the operation and development of high-speed railways in China [62,64].

Since people had a basic understanding of the principle of railway wheelset self-guiding motion related to wheel shape in the 19th century, the improvement of wheelset design has never stopped. From the early empirical design method to the widely used computer numerical optimization design method, railway scholars have been looking for wheel profile with the optimal relationship between wheel and rail, so as to fully improve the dynamical performance of locomotive and rolling stock. At present, the design of the wheel tread has achieved fruitful results [62]. Railway wheel tread used has successfully transferred from the earliest conical tread to the worn tread. However, there are still obvious limitations in the design of the worn tread and its application. So far, the expected functional indicators of the wheelsets, which were put into operation, cannot reach optimal at the same time. The multi-objective optimization technology for wheel–rail interaction is not so mature. Currently, the aim of the wheel tread design mainly improves a single performance parameter, such as the rail profile expansion method [64] and the normal clearance method of wheel/rail [65]. They can effectively improve wheel–rail rolling contact performance and reduce wheel–rail wear. However, the wheels designed using these methods contributed little to the improvement of vehicle dynamic behavior because the influence of vehicle suspension parameters was not considered in the design. The inverse design method of equivalent conicity or wheel diameter difference [66,67] mainly aimed at improving vehicle dynamics.

In the early years of China's high-speed railway operation, there were two main types of high-speed trains operating at speeds over 300 km/h. Due to their different suspension parameters, two different conicity wheelsets were used. One with relatively low conicity and relatively thin rims is called Wheel A for convenience. The other with relatively high conicity and relatively thick rims is called Wheel B. Considering the main purpose of applying the two conicity wheels at that time was to pursue the small wheel–rail wear and meet the requirement of better vehicle dynamic behavior only. The following problems appeared soon after the two types of wheels were used. The first common feature of their problems was that the wheelset equivalent conicity increased rapidly with increasing operating mileage, shortly after the new wheels (or just after repairing) in operation. The critical speed decrease in the vehicle hunting (at 1–2 Hz) caused by the conicity increase was faster than the designed or predicted target value. Another common feature was that the trains equipped with new wheels were very stable and comfortable when running on straight tracks at high speeds, and the wheel–rail contact light band (the running surface) was more concentrated. At this stage, the wheel wear was mainly concentrated around the nominal rolling circle, about a hollow wear of 30–40 mm. The depth of more than 50 percent of the wheel hollow wear was in 0.20 mm–0.25 mm [63]. For subway train wheels, heavy haul train wheels and train wheels on mixed passenger and freight transportation lines, the degree of such hollow wear should be said to be slight and normal, and it did not

even get much attention. However, when the train was running at a high speed (above 300 km/h), the running stability of the wheelset was very sensitive to such hollow wear. When the operating mileage was less than 100,000 km, wheelsets and bogies produced lateral sloshing at 7–10 Hz, and the train operation speed had to slow down. That is, such slight hollow wear on the wheels seriously affects the normal operation of high-speed trains. This phenomenon was more serious for the trains with Wheel B than for the trains with Wheel A. When the trains with Wheel A were running on the high-speed straight tracks with rails of minor improper wear at high speeds, the trains often wobbled at low frequencies (1–2 Hz). That time, this was also a problem that puzzled the normal operation of high-speed trains.

According to several years of testing and analyses on the wheel wear state of high-speed trains at operation sites and its influence on vehicle behavior, Cui et al. [62] proposed a new design method for a high-speed wheel geometric profile, which comprehensively considered common and individual problems in traditional wheel tread designs. The new design idea is indicated by Figure 17, in which there are two aspects of research and design. The first is the common design, which is usual and the main content of the traditional wheel/rail profile matching design. In the common part design, low contact stress between the wheel and rail is an important index to be pursued. Low contact stress can effectively reduce wheel–rail wear and rolling contact fatigue. A reasonable equivalent conicity of the wheelset can make the wheelset (or vehicle) have a higher critical speed of hunting and a better curve passing ability.

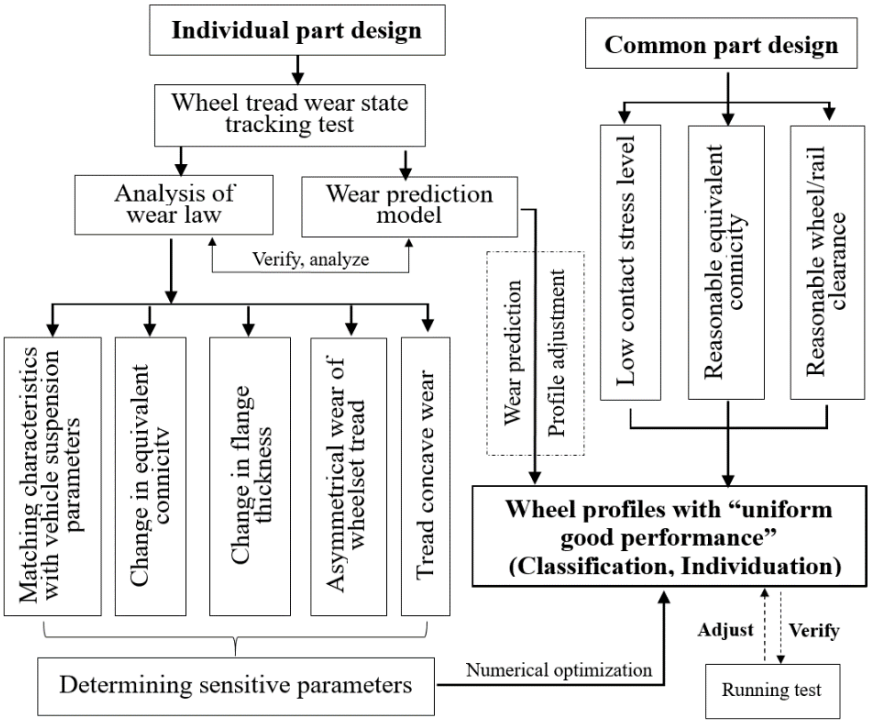

Figure 17. Design flow chart of high-speed wheel geometric profile.

In this part design, it is necessary to consider reasonable wheel/rail clearance. The reasonable clearance ensures that the wheelset conicity does not increase rapidly due to the hollow wear and prevents the wheelset from shaking at 7–10 Hz when running at high speeds. For the high-speed lines built, the track gauge has a 1435 mm+ allowable error. Usually, the clearance between wheel and rail can be changed by modifying the wheel rim thickness only. It effectively reduces the change rate of the equivalent conicity of the original (or new) wheelset (caused by the hollow wear increase). The performance of Wheel B can be improved effectively by reducing the rim thickness of Wheel B.

The individual part design in Figure 17 is also a key part of the research and design of high-speed wheelsets with outstanding performance. With the help of a large number of field wheel wear test data and their statistics analyses, the profile and geometric dimensions of high-speed train wheels in operation are optimized to improve their performance. The prediction analysis of the optimized wheel performance includes its wheel–rail rolling contact behavior, wear state and potential wear variation trend, influence on the vehicle-track coupling dynamic behavior, internal and complementary factors with vehicle suspension parameters, etc. To accomplish the above tasks, a complete set of theoretical models and corresponding numerical analysis methods are needed. They should include wheel–rail rolling contact model, wheel–rail material wear model, vehicle-track coupling dynamics model and wheel–rail tread matching optimization model. If the performance index of part of the wheel after optimization, predicted in theory, is not up to the standard, further optimization or multiple optimizations should be carried out to achieve the theoretical standard. Then, it is necessary to carry out real vehicle operation test verification after so many cycles (verification to optimization and improvement, and then verification) to achieve the most desired goal.

According to the design scheme shown in Figure 17, a new type of high-speed wheel tread was designed. Figure 18 indicates the equivalent conicities of the new designed high-speed wheel and Wheel B, and their hunting critical speeds with the increase in operating mileage. Obviously, the re-profiling interval of the new designed high-speed wheel increases by 30%. At the same time, in the range of the lateral wheelset deviation of less than 8 mm, the wheel/rail contact pressure of the new high-speed wheel is lower than that of Wheel B. In the operating speed range from 200 km/h to 400 km/h, the average wear work index of the new designed wheel is greatly reduced and the change in its wear work index is very small [62]. The design concept in Figure 17 successfully supports wheel MB10 design of a FUXIN high-speed train [68]. At present, the design of a subway train wheel profile is also on trial following Figure 17.

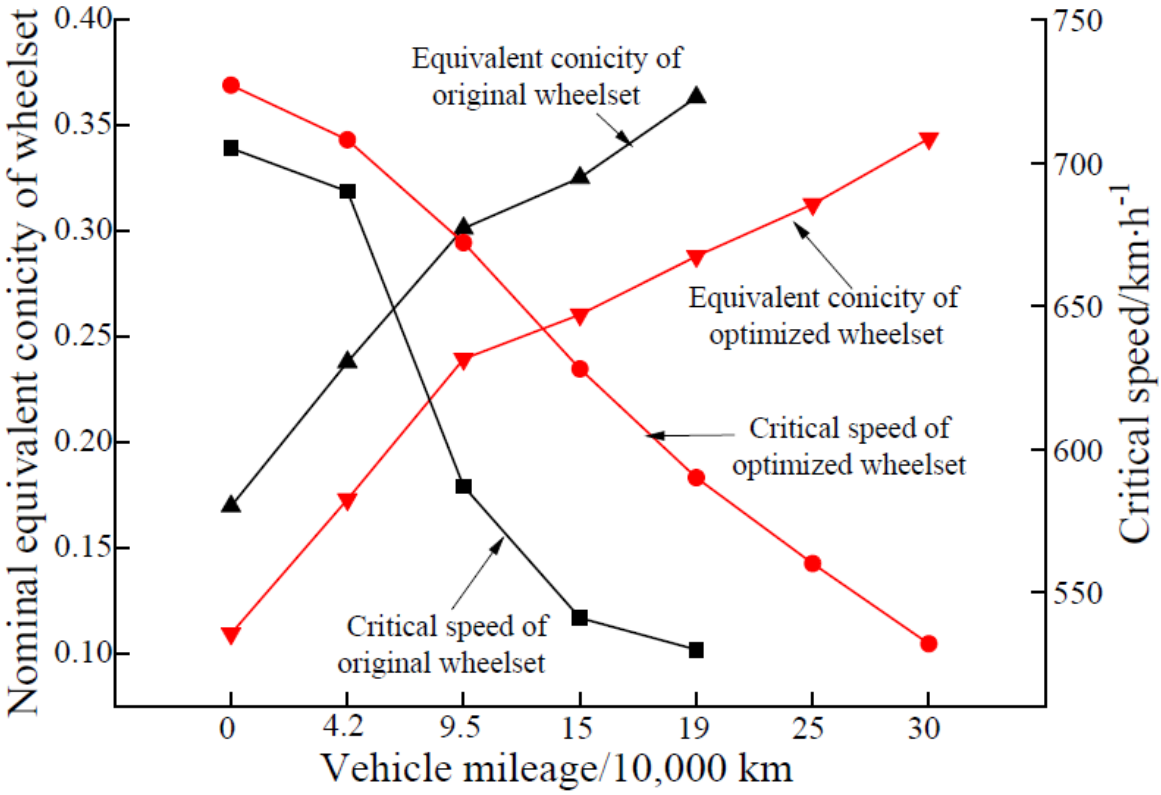

Figure 18. Equivalent conicities and critical hunting speeds of old and new wheelsets with operation mileage.

Optimal matching of wheel and rail materials is the other key problem. It includes two aspects of research content. One is the suitable hardness ratio of wheel material to rail material, and the other is the proper hardness and toughness of wheel/rail material itself. Optimal matching of wheel and rail materials can effectively prevent wheel/rail wear and rolling contact fatigue. Wheel/rail wear and fatigue crack are the main damage states in service. Figure 19a indicates the serious pit wear (called hollow wear) on the lateral tread of the wheel (working face) and wheel flange wear. This kind of wear state causes the critical speed of stable operation of the vehicle to decrease greatly, and its performance through the curved tracks becomes poor. Figure 19b denotes wheel tread spalling and flange root checking. They will lead to high-frequency contact vibration and noise of the wheel and rail and seriously cause wheel breakup, lead to derailment accidents.

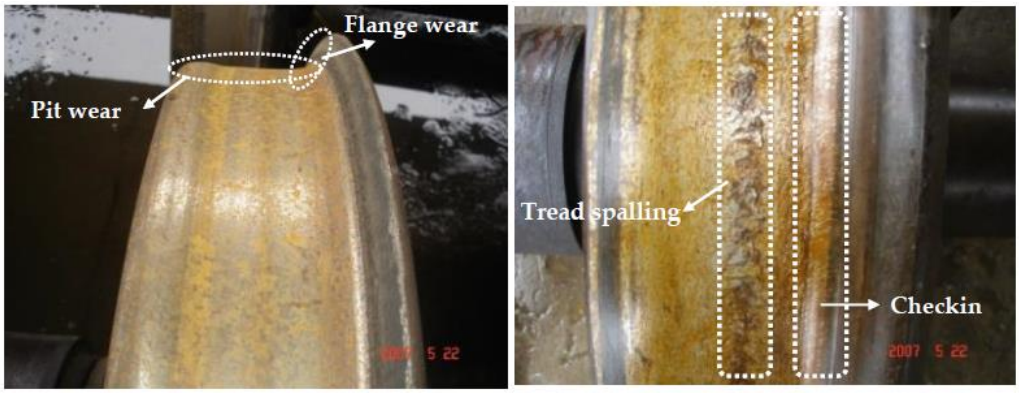

Figure 19. (**a**) Serious pit wear on the lateral tread of wheel; (**b**) wheel tread spalling and flange root checking [16].

What is the suitable hardness ratio of wheel material to rail material? The correct answer is related to the balanced development of wheel/rail wear and their mutual adaptation, which ensures the excellent dynamic performance of trains in long operation processes. It is also related to the low operating cost. For high-speed rail in Japan, the hardness ratio of wheel–rail materials is about 1.2. In Europe, the hardness ratio is 0.94–1.07, and 0.94–0.98 for China's high-speed railway [69]. The selection and practical use of these ratios are basically based on experience, without strict engineering scientific test verification and theoretical analysis data demonstration. The optimal value of the ratio has not yet been found. Its choice is also controversial in the rail industry. At present, there are no good methods nor ideas to find its best value.

There is a traditional view or experience in railway operation and maintenance. That is, the repair and replacement of wheels are much more convenient and cheaper than rails. It is generally recommended to use wheel material hardness, which is slightly lower than that of rail material. Researchers from Southwest Jiaotong University used the small-scaled wheel–rail test device to test the wear of high-speed wheel–rail materials under rolling and sliding states. Figure 20 shows the change in total wear amount of wheel/rail specimens with different material hardness [70]. A disk-simulating wheel was considered as a driving disk in the test device and the other disk-simulating rail was a driven disk. It was found that the total wear amount of the wheel/rail materials was the lowest when the hardness ratio of the rail/wheel specimens was about 1.05. The curve in Figure 20 was fitted into a unary quadratic polynomial. This interesting phenomenon suggests whether different hardness should be applied to locomotive wheel materials and trailer wheels. If so, this obviously increases the cost of wheel manufacturing and operation maintenance.

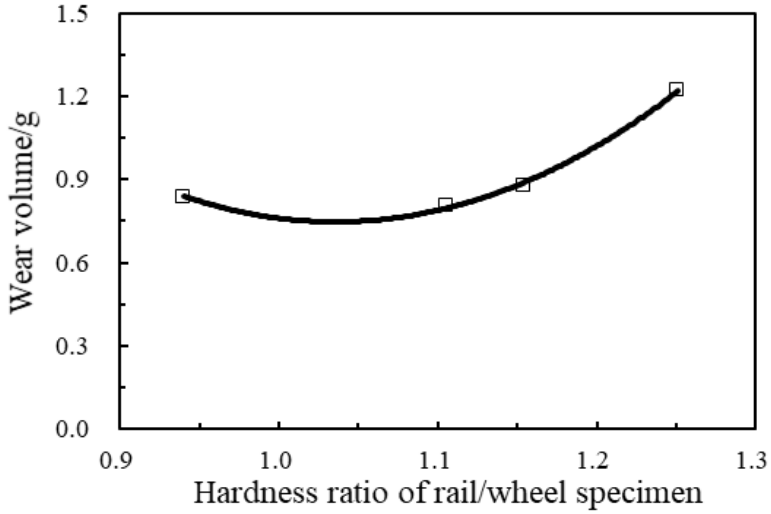

Figure 20. Total wear volume of wheel/rail specimens vs. hardness ratio of wheel material to rail material.

Figure 21 shows a schematic diagram of working hardening and frictional wear of materials of wheel–rail contact surface. The vertical axis on the right represents the hardness of materials of the wheel–rail contact surface, the horizontal axis N_R represents the number of wheel/rail rolling contact, the red curve $Y_m(N_R)$ represents the nominal hardness function of the contact surface materials, the blue curve $Y_s(N_R)$ represents the actual hardness function of the materials, $Y_s(N_R)$ is lower than $Y_m(N_R)$ because the wheel/rail contact surface materials are constantly worn away, Y_0(HB) is the initial hardness of wheel/rail surface materials, h_W (N_R) is the wear depth of the contact surface and K in the Figure represents the intersection point of the wear depth and the actual hardened layer depth. When the wear depth is equal to the hardened layer depth, if the wheel/rail continue to roll slip wear, the wear will increase rapidly.

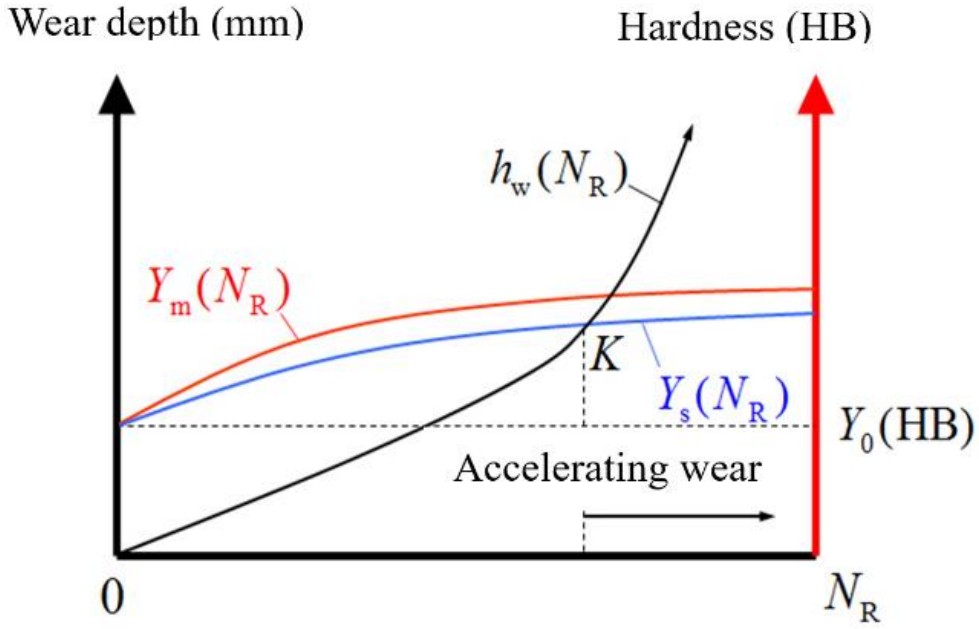

Figure 21. Hardness and wear of wheel/rail contact surface material vs. number of wheel/rail rolling extrusion.

There are two more important factors to consider in wheel/rail material selection. The first consideration is that, for operating on the same line, the number of rolling extrusions of wheel material is different from the number of rolling extrusions of rail surface material, then the wheel wear and the rail wear are different every day. If the influence of the

difference in the wheel–rail material properties on the wear of the wheel and rail is not considered, the ratio of the average wear of each wheel to the average wear of the rail in operation on the same line is expressed by formula (3). If calculated according to formula (3), the daily wear of the wheel on a certain line is usually dozens of times that of the rail. Considering the factors discussed above, determining the hardness ratio of wheel material to rail material is really a difficult problem to study.

$$\frac{\text{Average wear of wheel}}{\text{Average wear of rail}} \approx \frac{\text{Number of turns of a wheel rolling on a rail each day}}{\text{Total number of wheels rolling on a rail each day}} \quad (3)$$

The second consideration in choosing wheel–rail materials is the appropriate hardness and the appropriate toughness of the material itself. The high hardness and high toughness of wheel/rail materials themselves can resist effectively wear and rolling contact fatigue. However, in general, the requirement for both high hardness and high toughness of metallic materials is difficult to be satisfied. Improving the hardness of the material, that is, increasing the yield strength of the material, can effectively improve the wear resistance of wheel–rail contact surface, but for the high hardness of the material, its toughness is difficult to meet the requirement of crack resistance development. Therefore, to improve the performance of wheel/rail materials, it needs to improve its hardness and toughness at the same time, that is, in choosing wheel and rail materials, their hardness and toughness need to be guaranteed at the same time.

At present, the wheel/rail material selection can only be made by means of extensive practical experience and reference to test results of laboratory test equipment. The basic idea is to carry out the test simulating a wheel rolling over a rail with a pair of rollers, namely disc to disc. During the test, test specimen materials with different toughness and hardness are changed, and the sliding and normal contact force of two discs are set close to the actual situation of the wheel–rail in service, and rolling–sliding test is carried out under different mileage conditions. The test results should show the following three situations: (1) if the crack and exfoliation on the contact surface of the specimen are serious, the hardness of the material is too high to be used. (2) If there is no crack and the wear is too severe, the material is too soft or has too high of toughness. The hardness is not enough and should not be used. (3) If the crack position is constantly changed with the increase in the test mileage due to wear, and also the length and depth of the cracks are not large, the toughness and hardness of the material are appropriate or balanced. This kind of material basically meets the requirement and may be recommended to use. So far, no research results have been published in this respect. It is obvious that there are the following deficiencies in the selection of metal materials for the wheel and rail by the above test method. If the material properties of the wheel and rail are not different, their wear amount is not different in every rolling contact. The hardness change in the wheel and the rail in actual operation is different from that of the test specimens. The test environment is also different from the fields, including the effect of the attachments. Interaction mechanism of fatigue crack and wear on wheel–rail rolling contact surface reproduced by the test process is not quite the same as the situation in the field. At present, the best match of hardness and toughness of wheel/rail materials has not been found. Only efforts can be made to improve the hardness and toughness of wheel/rail materials at present.

4. Adhesion Theory and Mechanism of High-Speed Wheel–Rail in Rolling Contact

Wheel–rail adhesion is an important factor affecting the safety and efficiency of train operation. Especially for high-speed trains in operation, the requirements for high-acceleration and high-deceleration capacities are becoming increasingly high, and the traction and braking forces between the wheel and rail rely on the property and level of the adhesion in the wheel/rail contact patch. Therefore, it is particularly important to explore the key factors affecting the property and level of wheel/rail adhesion in rolling contact at high speeds. The ratio of the longitudinal tangential force to the normal pressure between

the wheel and rail is defined as the adhesion coefficient by the railway industry. It is taken as an important parameter to measure wheel–rail adhesion characteristics.

The adhesion coefficient is mainly related to the friction caused by wheel–rail contact surfaces. It is affected by wheel–rail material properties, contact surface states, contact surface attachments, vehicle operating conditions, environmental conditions and so on. In the past, research on the influence of these factors on wheel–rail adhesion characteristics mainly relies on experimental methods. China's large-scale high-speed railway operation and the statistical analysis of field test data shows that the adhesion characteristics at less than 350 km/h under dry conditions can satisfy the traction and braking of the train well. The real impact on the adhesion is the contact surface state and the attachments on the contact patch. These attachments include rain water, dew, water pollution caused by fog, oil pollution caused by oil leakage from vehicles and engineering equipment, fallen leaves, contact surface rust and oxidized metal abrasive particles. In recent decades, scholars have focused on the analysis on the influence of the attachments on the adhesion characteristics. Although some progress has been made, the problem of wheel/rail adhesion cannot be solved satisfactorily. Ohyama T. and his collaborators made outstanding achievements in experimental research. They systematically studied the influence of surface state and operating parameters on the adhesion characteristics by means of a small-scale double-disk rolling test device [71,72]. Zhang W. et al., Gallardo-Hernandez, Lewis, Wang, Arias-Cuevas, Li et al. and Olofsson et al. studied the wheel–rail adhesion characteristics under oil lubrication or water lubrication by using full-scale or reduced-scale rolling devices, respectively [73–79]. The adhesion coefficient distribution in the speed range of 30–270 km/h was obtained through the tests under the condition of water spraying on the track of Japan Shinkansen [18,80], and the relation function between the adhesion coefficient and the operating speed was fitted by using the test data.

Chang et al. used 1:1 high-speed wheel–rail test device (as shown in Figure 22) to reproduce the characteristics of the wheel–rail adhesion coefficient. In the test, they considered the influence of different wheel–rail interface roughness levels, axle loads, wheel–rail interface water volumes, wheel–rail creepage levels and ambient temperatures on the adhesion characteristics. The test speed reached 440 km/h. Figure 23 shows the test results. It indicates the variation in the adhesion coefficient with the operation speed, different roughness levels and water mediums [81].

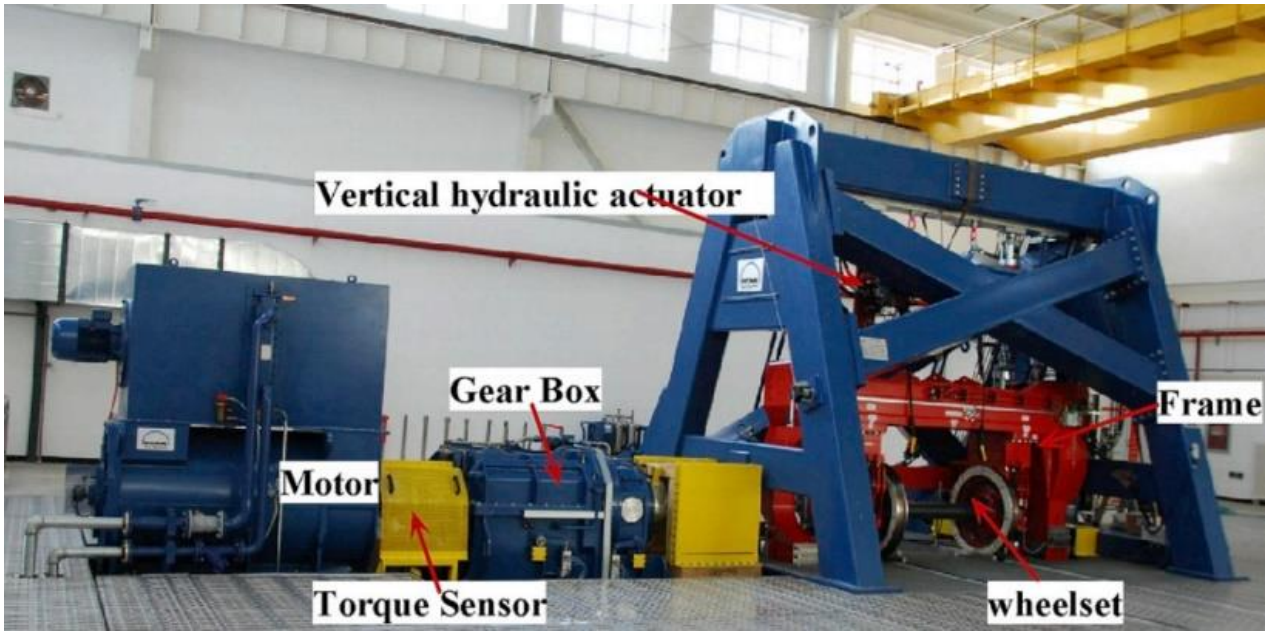

Figure 22. The 1:1 high-speed wheel–rail test device.

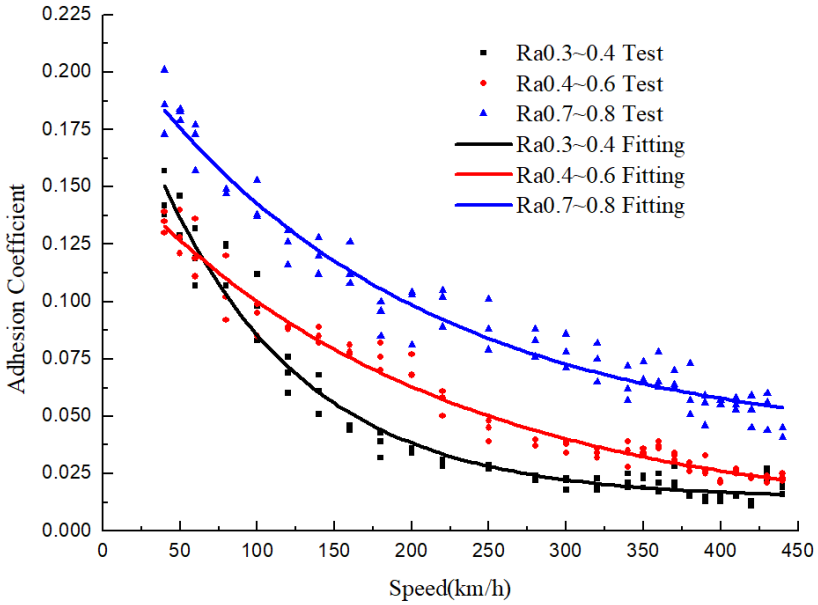

Figure 23. Adhesion coefficient with velocity at different roughness levels and water mediums [81].

In the test of Figure 23, the axle load is 17 tons, the wheel–rail creepage is set at 2% and the amount of water sprayed on the wheel–rail contact surface is 300 mL/m. In Figure 23, Ra denotes the roughness level, the symbols ▲, ● and ■ represent the test results at different roughness levels and solid lines with different colors represent their fitting results. For water pollution and the three roughness levels, as the test speed increases, the wheel–rail adhesion coefficient decreases rapidly. The decreased rate of the adhesion coefficient is almost the same for the two higher roughness levels. For the lowest level roughness (the contact surface is relatively smooth), the drop rate is the largest in the range of 50–200 km/h. The reason is that for the lower roughness level of the contact surfaces (or relative smooth surfaces), the water mucous membrane on the wheel–rail interface is easier to form with the rolling speed increase. In the situation, the solid contact ratio between wheel–rail interface decreases rapidly, and the contribution of solid friction to the tangent force decreases rapidly. This leads to the rapid decrease in the wheel–rail adhesion coefficient. These results have an important value for evaluating wheel–rail adhesion level, safe operation and rational adhesion utilization of higher-speed trains in service.

Due to the complexity of wheel–rail in rolling contact and many factors affecting the adhesion coefficient, the establishment of a physical model and numerical method is still a challenging problem. This problem is related to the research on the influence of attachments between wheel and rail, micro-roughness of the contact surfaces and material nonlinearity. Therefore, the research progress in this area is particularly lagging behind. At present, elasto-hydro-dynamic lubrication theory and microscopic solid contact theory are widely used to analyze the adhesion characteristics. Figure 24 indicates the physical model of wheel–rail adhesion taking into account such factors as the elastic fluid between wheel and rail, wheel/rail elastoplastic microscopic roughness, wheel rolling speed, etc. Figure 24a indicates that a power wheel rolls on a rail at speed v with drive torque T and vertical load P. So, the adhesion force between the wheel and the rail is F. Figure 24b,c show the geometric amplification of the wheel–rail contact area. They describe the microscopic roughness amplitude (δ_1, δ_2) of the contact surfaces and the fluid between the wheel–rail interface, respectively. Figure 24d shows three texture states of rough surface ($\gamma < 1$, =1 and >1). $\gamma < 1$, =1 and >1 represents the distribution state of roughness texture along longitudinal, longitudinal and transverse and lateral directions, respectively. This wheel–rail contact state seriously affects the wheel–rail adhesion coefficient or wheel–rail adhesion force F.

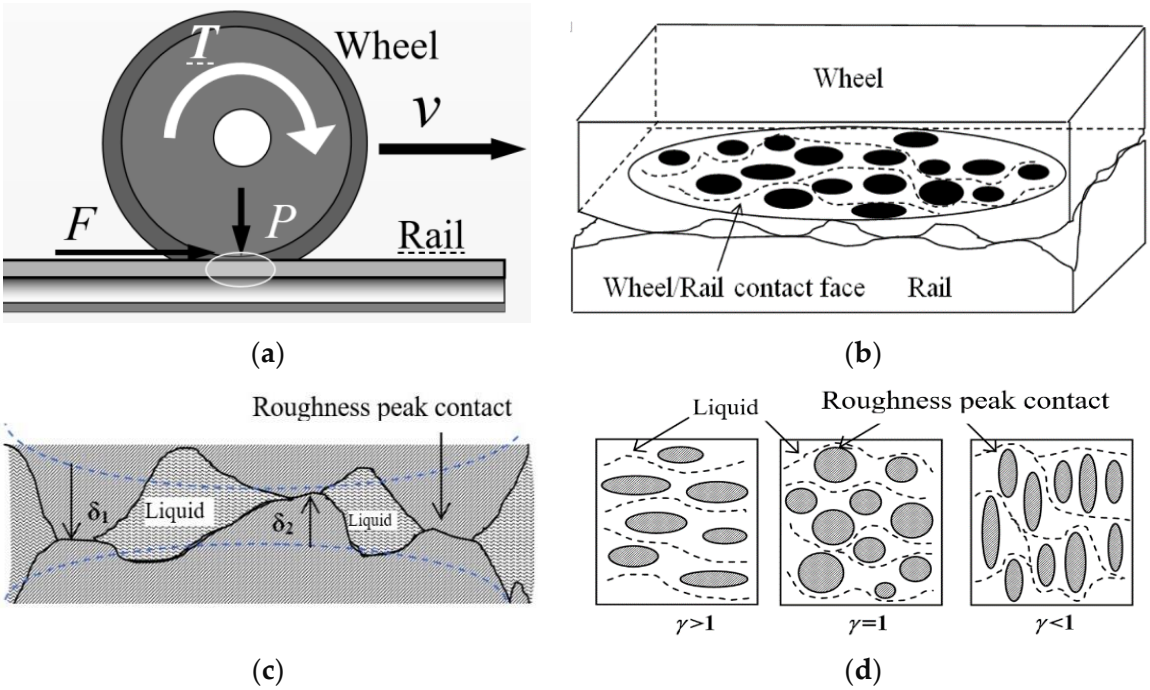

Figure 24. Adhesion physical model considering the effect of elastic–fluid and elastoplastic micro-roughness between wheel and rail and wheel rolling speed.

According to Figure 24, Ohyama T. first introduced the elasto-hydro-dynamic lubrication theory into the study of wheel–rail adhesion and theoretically studied the adhesive characteristics of the attachments on the rough surfaces of wheel–rail [82]. Chen H et al. found that wheel–rail surface roughness and temperature have a great influence on the adhesion coefficient by using a simplified model and compared the calculated results with the measured results on Japanese Shinkansen, and the results were in good agreement [83]. This model is a mixed lubrication model established on the basis of the Grubin theory.

Wu B et al. developed a two-dimensional numerical model. The numerical method adopted "the Multi-grid Method" with better stability in the numerical iteration. Using it obtained the wheel–rail adhesion characteristics in a water medium and oil medium at higher speeds (up to 500 km/h). The influence of roughness parameters, axle load and operation speed on the adhesion coefficient was analyzed in detail, and the variation characteristics were explained from the quantitative point of view. The numerical results are in good agreement with the experimental results. In addition, they also analyzed the influence of the different physical properties of water and oil on the adhesion characteristics. They found that the adhesion coefficient decreased faster than that of water in the presence of oil pollution on wheel–rail surface, and explained the causes from the numerical point of view [84–86]. Chen H et al. developed a three-dimensional calculation model using the mixed lubrication theory to numerically analyze the adhesion characteristics in a water medium. It was found that speed, water temperature and surface roughness had great influence on the adhesion coefficient. In the calculation, they considered the effect of the size parameters of a small-scale testing machine. Finding the numerical solution needs to avoid the small film thickness ratio and the numerical stability problem caused by the extreme working conditions (film thickness is negative), which is related to wheel–rail contact. In addition, the simulation condition of the point contact is different from the actual wheel–rail elliptic contact patch [87]. The obtained result has theoretical significance, but the prediction of actual wheel–rail adhesion needs careful consideration. To this end, Wu B et al. extended their two-dimensional model to a three-dimensional model [88]. The geometric dimensions and actual normal load at the wheel–rail contact point of a CRH2 high-speed train were considered in modeling and analyzing. The variation in the

adhesion coefficients with operation speed, wheel/rail contact surface roughness, axle load and other factors were obtained. The calculated results are in good agreement with the experimental results.

The numerical models discussed above are all aimed at the existence of a single medium between wheel and rail, and there may be more than two or more mixed media on the actual wheel–rail contact surfaces. Therefore, Wu B et al. established a wheel–rail adhesion model with a water and oil mixture [88,89]. They believed that the difference between water and oil is mainly in viscosity, and considered that the wheel–rail surface roughness level and the thickness of water–oil film were basically in the same order of magnitude. It was assumed that water and oil are stored in segments in the surface bulge between the wheel and rail, and a unified equation was used to solve the solution of the whole contact area. The adhesion coefficient they obtained is somewhere between the results when considering the effects of water and oil alone. It is in good agreement with the current experimental results. However, the longitudinal interaction of the water–oil medium is neglected in their study. In practice, large longitudinal slippage between wheel and rail is inevitable during traction and braking, which can lead to an increase in temperature and influence the adhesion coefficient. Therefore, their theoretical model needs further improvement.

Through experiments and numerical analysis, Chen H. found that the influence of water temperature on the wheel–rail adhesion coefficient could not be ignored [90]. However, there is, so far, no numerical model which can take temperature-rise, rheology, micro-roughness and elastoplastic deformation into account at the same time. To simplify the model, on the basis of Chen's simplified model, Wu B et al. [89] considered the friction temperature-rise between solid rough peaks in the inlet region of the contact patch and the elastoplastic contact between microscopic rough peaks proposed by Zhao Y et al. [91] at the same time. The variation in the adhesion coefficient with and without the influence of heat was calculated. The numerical result obtained is shown in Figure 25. Obviously, the numerical result considering the thermal effect is closer to the actual experimental result. Meanwhile, the distribution of the wheel–rail adhesion coefficient under the influence of multi-factor coupling was investigated, as shown in Figure 26. It can be found that the roughness level of wheel/rail contact surface and the operation speed have a great influence on the adhesion coefficient, which is similar to the characteristics shown in Figure 23.

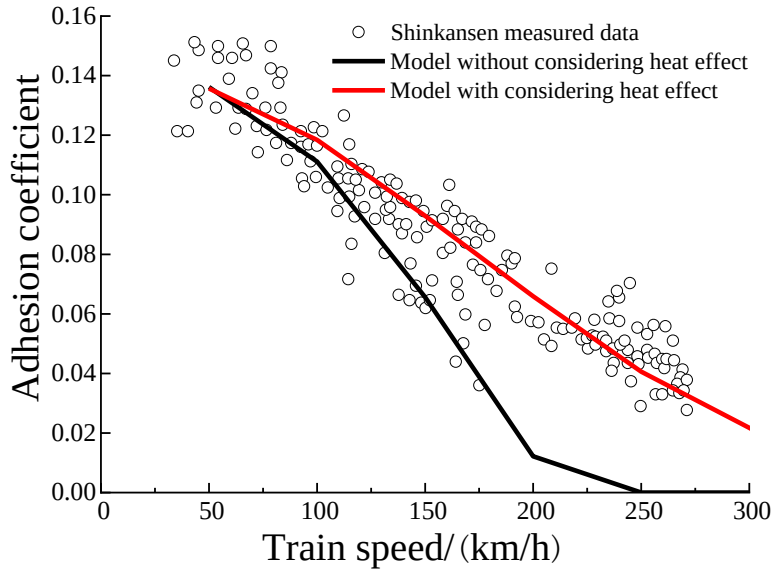

Figure 25. Comparison between experimental results and numerical results with considering thermal effect.

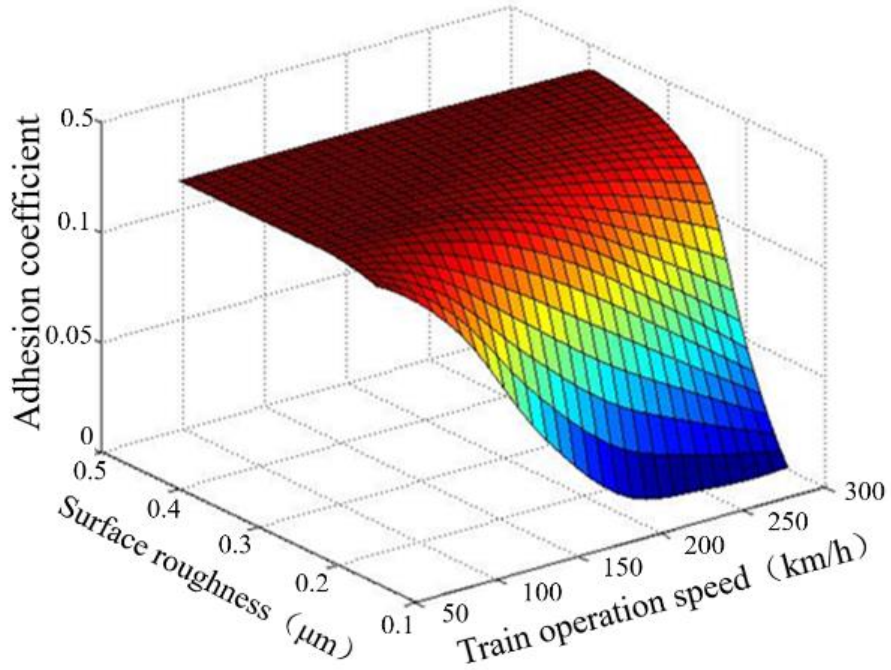

Figure 26. Influence of operation speed and surface roughness level on adhesion coefficient.

Recently, studies on the characteristics and mechanism of high-speed wheel–rail adhesion have considered the vehicle-rail coupling system and the problem of adhesion-induced damage. Based on the high-speed wheel/rail adhesion experiment, Wu et al. [92] generalized the application of the functional friction coefficient parameters of Polach in the water medium suitable for high-speed conditions, modified the simplified FASTSIM theory, and conducted the numerical simulation of high-speed train traction with large sliding. The attrition and fatigue characteristics of wheel/rail under large traction sliding were investigated preliminarily. Combined with the vehicle/track coupling dynamic model and the deterministic mixed lubrication model, Wu et al. [93] established a new high-speed wheel–rail adhesion dynamic model of the high-speed train passing over a curved track in the presence of a water medium. The model also considered the effects of starvation oil and measured three-place roughness on wheel–rail adhesion. The transient adhesion characteristics at different speeds were obtained.

The application of friction modifiers has been recognized as a promising emerging tool in railway engineering to mitigate wheel–rail interface deterioration, energy consumption, vibration and noise by modifying friction to the level which is required to increase the wheel/rail adhesion coefficient under consideration of adverse friction conditions. Yang et al. [94] experimentally investigated the effects of two types of top-of-rail friction modifiers and their application dosages on wheel–rail dynamic interactions with a range of angles of wheelset attack using an innovative well-controlled V-track test rig, as shown in Figure 27. The research results promote the technical performance improvement and application of friction modifiers and improve the dynamic action of wheel and rail.

Although some wheel/rail adhesion mechanisms have been clarified by using experimental and numerical methods, the actual wheel–rail contact behavior is very complex and influenced by many factors. The following problems still need to be solved in experimental and numerical simulation aspects: (1) the numerical convergence in the presence of a water medium with a small film thickness ratio; (2) a more accurate numerical model considering the influence of multi-factor coupling (temperature, micro-roughness, elastoplastic contact with liquid, rheological sand, leaves and other pollutants) on the adhesion coefficient; (3) numerical simulation of real geometrical characteristics of micro-roughness; (4) in the process of high-speed wheel–rail adhesion test, the influence of the change in the real geometric characteristics of micro-roughness on the adhesion coefficient due to rolling and

wear of wheel–rail; (5) experimental and numerical modeling of new viscosifiers between wheel and rail at higher speeds. Only in this way can we estimate the change law of wheel–rail adhesion more effectively and accurately and provide a theoretical basis for the measures to improve the adhesion coefficient of high-speed wheel/rail system, so as to ensure the safety of high-speed train operation.

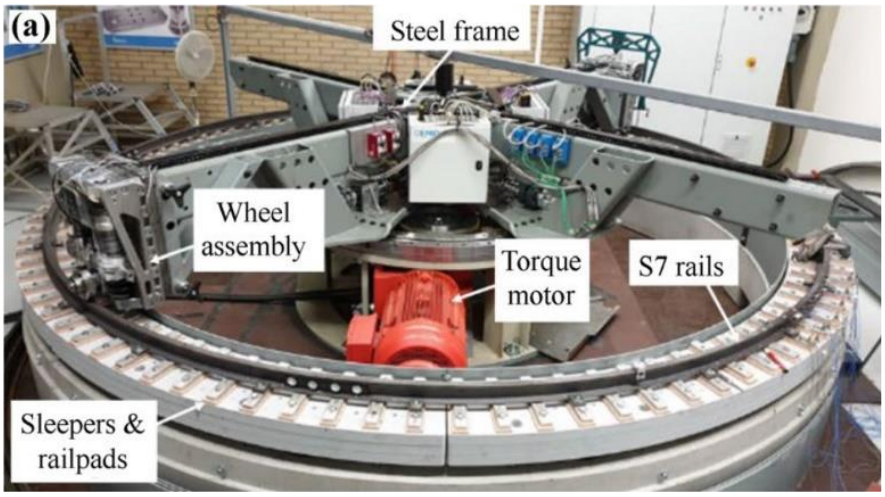

Figure 27. V-track test rig [94].

5. Wear and Rolling Contact Fatigue of High-Speed Wheel–Rail

5.1. High-Speed Wheel/Rail Wear

5.1.1. Transverse Wear of Wheel/Rail

The main problem of damage of high-speed wheel/rail is wheel/rail wear. Rolling contact fatigue is not as serious as the lines of metro, freight and mixed passenger/freight. Wheel/rail wear mainly includes the transverse wear on wheel/rail treads and the uneven longitudinal wear (along with wheel/rail running surfaces). The transverse wear of wheel/rail directly affects high-speed train stability, which shows 1–3 Hz hunting motion of the car-body and 7–10 Hz hunting motion of the bogie or wheelset, respectively.

In the early operation stage of China's high-speed trains, the transverse wear of the wheel was mainly manifested as the severe wear of the wheel rim and the hollow wear at the nominal rolling circle of the wheel. They were the common behaviors of railway wheels. When the wheel rim wore off 1 mm, through the re-profiling to restore the original wheel profile, it was necessary to cut off the wheel radial height of about 3 mm. It greatly shortened the service life of the wheel. In addition, serious rim wear led to wheelset conicity to change, which caused low-frequency shaking of the vehicle body. Wheel rim serious wear was caused by the serious friction wear that occurred between the wheel rim and the high rail of sharp curved tracks when the train passes through the sharp curved tracks (radius of about 300 m) into the depots. At the same time, it also caused serious wear of the inner corner of the high rail. Serious wear of the wheel rim and rail corner was reduced through lubrication and optimization of the geometries of sharp curved tracks [65].

The hollow wear at the nominal rolling circle of high-speed wheels is as shown in Figure 28 [9,63]. In the figure, r_{l1}, r_{l2}, r_{r1} and r_{r2} are the rolling radii at four different points on the left and right wheel treads, located on both sides of the hollow wear; $\boldsymbol{y}$ is the lateral displacement of the wheelset center with respect to the track central line. Statistical analysis of field test data shows that 50% of hollow wear of high-speed wheels have the depth of about 0.15–0.25 mm, and the width is about 30 mm–60 mm, depending on the operating mileage. The hollow wear center is close to the wheel nominal rolling circle. When a train was running at high speeds, the transversal oscillation of bogie and wheelset at 7–10 Hz was very sensitive to the hollow wear of the wheelset, as shown in Figure 28. Faced with the bogie transversal oscillation increasing the horizontal acceleration level of the axle box, the train operation at high speeds had to slow down. The solution of this problem puzzled

railway engineering experts for some time. However, it is not difficult to understand the mechanism of the hollow wear formation on high-speed wheelsets, as shown in Figure 28, which leads to the wheelset hunting motion of 7–10 Hz. When the hollow worn wheelset rolls over a pair of rails, if the heads of the two rails are lightly flattened due to wear or the radii of the arcs of the rail heads become larger, the two-point contact forms between the wheel/rail on each side. In this case, a small lateral wobble as the wheelset rolls along the track at high speeds will result in discontinuous or jumping changes in the instantaneous rolling radii of the left and right wheels. Then, the change in diameter difference between in the left and right wheels, or equivalent conicity of the wheelset, is discontinuous with y, and they change periodically and reversely. From Figure 28, the radius difference is written as $\Delta r_i = r_{ri} - r_{li}$ (i = 1, 2) and the equivalent conicity is written as $\lambda = |\Delta r_i|/2y$. If the lateral displacement y <0, the subscript i = 1, and if y > 0, i = 2. Usually, $r_{l1} < r_{l2}$ and $r_{r1} > r_{r2}$ or they are not equal. The longitudinal creepages and the longitudinal creep forces between the left and right wheels/rails depend on the radius difference Δr_i. Their variation characteristics with y are similar to that of wheel diameter difference. The longitudinal creep forces on the left and right wheels form a moment of couple that will alternately excite the periodical yaw motion of the wheelset at 7–10 Hz [63].

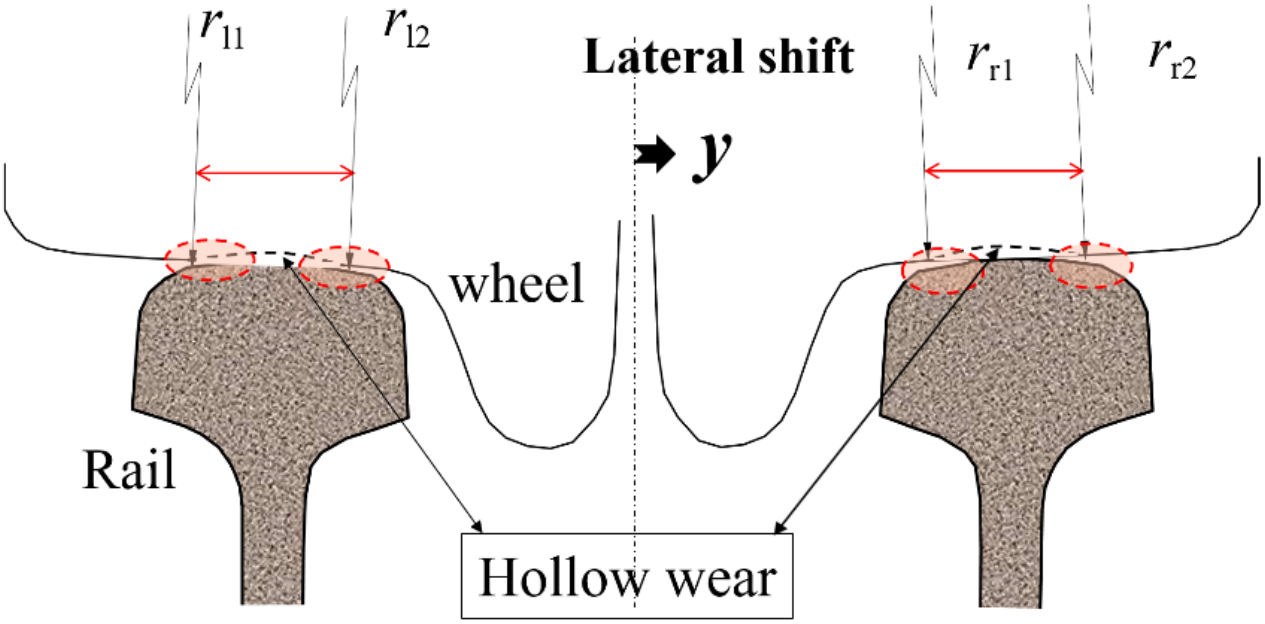

Figure 28. Hollow wear of high-speed wheelset.

The following measures can be used to effectively solve the above problem. (1) Using the rail with a more convex head rail (60N rail on trial) or by grinding to eliminate the two-point contact formation that may result from the case of wheel hollow wear at the wheel/rail tread; (2) under the condition of ensuring the vehicle stability, on the same track line using more than two profiles of rail head can produce the uniform wear on wheel tread through wheel/rail interaction; (3) further optimizing the wheel profile. The rate of hollow wear can be effectively reduced by appropriately reducing the conicity of the tread close to the root of the wheel rim. It is performed by reducing the wheel rim thickness in the wheel optimization. The optimized new high-speed Wheel Mb10 is a successful application case [63].

5.1.2. Uneven Wear in the Rolling Direction of High-Speed Wheel/Rail

Uneven wear of high-speed wheel/rail in the rolling direction includes wheel out of roundness wear (called polygonal wear), rail corrugation and other irregular wear in the rolling direction. Firstly, the characteristics and the forming mechanism of the polygonal wear and the measures to suppress the polygonal wear development are discussed. After

a long-term tracking test and analysis of roundness wear of high-speed wheels at sites in China, it was found that polygonal wear phenomenon was relatively common. The out of roundness wear pattern was mainly reflected in the following forms: (1) Eccentric wear, also called the first-order polygon wear, was mainly caused by the excitation of the initial geometric eccentricity and the mass eccentricity of the wheel. (2) Triangle wear and polygonal wear of high-order were mainly caused by the first-order bending resonance of the wheelset and high-order bending modes of the wheelset and other factors. (3) Crescent-shaped wear might be mainly caused by braking or acceleration or skidding, which might cause large local wear on the wheel rolling circle. (4) Higher-order (greater than 14-order) polygonal wear is shown in Figure 29. Figure 29a shows the photo of a high-speed wheel with order 23 polygon wear [9,95]. Figure 29b represents the measured result of the polygonal wear in polar coordinates, as indicated by the black curve shown in Figure 29a. In Figure 29b, the red curve denotes the wheel radius variation along the wheel rolling circle after the re-profiling of the polygonal worn wheel. The valley-peak depth of the polygonal wear is from 0.03 mm to 0.2 mm. The wheel radius is 860 mm and the operating speed is 250 km/h. The wheel–rail contact vibration frequency caused by the polygonal wear is about 590 Hz. Such severe polygonal wear caused the high-frequency additional dynamic load between wheel and rail, which was more than twice the static load of the wheel and rail.

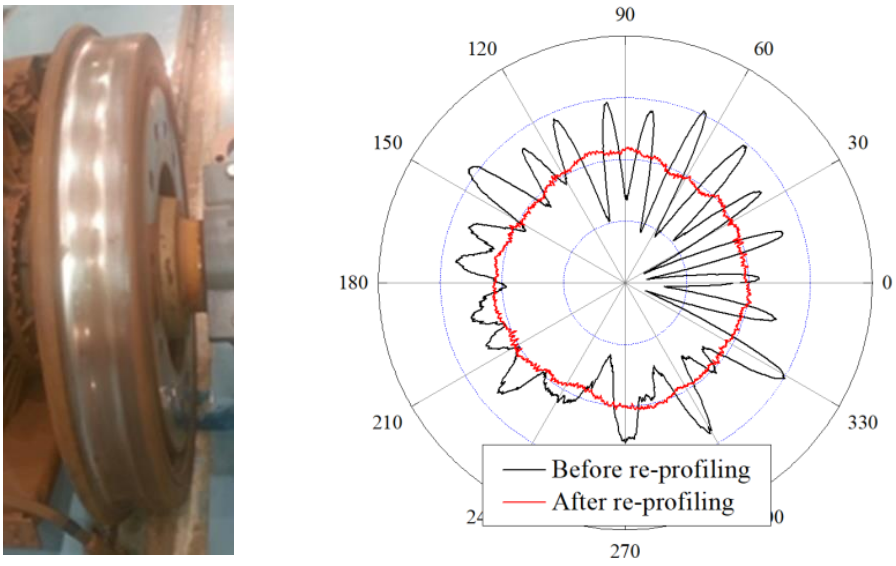

Figure 29. (**a**) Photo of polygonal wear of a high-speed wheel; (**b**) comparison of roundness of polygonal worn wheel before and after repair.

According to the statistical analysis of the field test data, the order of the polygonal wear of existing high-speed wheels in China (200–300 km/h) was mainly distributed in the range from 13 to 28. It led to the increase in noise level in the carriage by more than 10 dB [96]. The development of the polygonal wear led to the damage of some key parts of the train and track system, such as the fracture of connecting bolts of bogie parts and the elastic clip fracture of track fasteners [9,97].

One of characteristics of the polygonal wear is that the uneven wear mainly contains two wavelengths: a primary wavelength (corresponding to higher order and short wavelength) and a secondary wavelength (low order and long wavelength), which are about twice as related, as shown Figure 30. The black curves in Figure 30 represent the order spectra of the polygonal wear roughness level. The peaks appear at order 14 and 23, respectively. Their corresponding vibration frequencies are 400 Hz and 590 Hz, respectively. The mean peak-to-trough amplitude of the 23-order polygonal wear is much higher

than that of the 14-order polygonal wear. The polygonal wear of order 23 dominates in the polygonal wear. The peaks at point A in Figure 30 denote the eccentric wear of the wheels. Another characteristic of the polygonal wear is that the order of the polygonal wear decreases with the decrease in the wheel diameter due to the nature wear caused by wheel/rail interaction and the wheel re-profiling. Typically, for high-speed wheels of 920 mm diameter, if the polygonal wear occurs during their whole service life, there will be three high-rate development periods of the polygonal wear. Their whole lifetime is approximately 2 to 2.5 million km of operating mileage [97].

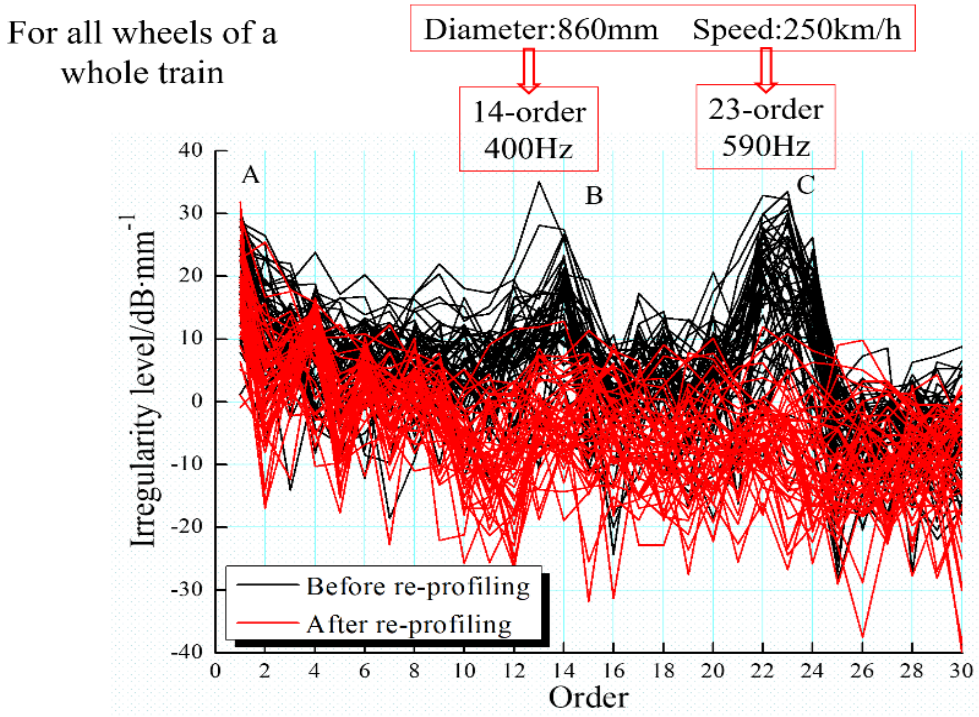

Figure 30. Irregularity spectra of the polygon wear of the wheels of a whole high-speed train. (**A**). the eccentric wear of the wheels. (**B**). 14-order 400 Hz (**C**). 2-order 590 Hz.

After many tests of field and laboratory and theoretical modeling analysis, the feature and mechanism of the polygonal wear are summarized as follows: when a train is running at high speeds, the wheel/rail system is excited by many factors (such as the irregularities of wheel/rail rolling contact surfaces, wheel mass eccentricity, track geometric parameter excitation, etc.). The excitation causes the vibration of the vehicle and track system, and the partial resonances of the system are excited. When the speed (v), wheel rolling circumference (C) and excited resonance frequency (f) meet a basic condition, the polygonal wear will be induced and develop rapidly. The basic condition is that the circumference (C) of a wheel can be divisible or approximately divisible by the vibration wavelength ($\lambda = v/f$). The formulization is that $n = C/\lambda$; here, n is required to be an integer or approximate integer is defined as the order of the polygonal wear. The question is whether the structural system resonances, related to the polygonal wear characteristics (order), come from the vehicle system or the track system or their coupling? The understanding of this has not been consistent so far [97].

Based on a large number of field tests and statistical analyses of data, theoretical and numerical simulation and experimental investigation and analysis by using 1:1 test device in laboratory [98–100], it was found that the structural resonances, related to the polygonal wear, came from the bogie frame and the wheelset, as shown in Figure 31. Figure 31a shows the two mode shapes of the bogie frame. Their frequencies are 585 Hz and 595 Hz, respectively, closest to the passing frequency of the polygonal wear shown in Figures 29 and 30. They were measured by using the laser testing system in the free

state of the frame. Figure 31b shows the fourth-order bending mode shape of the wheelset calculated by using the finite element method. The mode frequency is about 610 Hz. It should be noted that if the frame and the wheelset are in service, the modes and the corresponding frequencies discussed will change a little bit due to the constraints of the system structure and loading. In high-speed train operations, the modes of these frequencies are excited and they can cause the bogie system resonance. The resonance is transmitted to the wheel–rail rolling contact surfaces and can cause uneven wear of the wheel along the wheel circumference. If the resonance frequency meets the basic condition for the formation and development of the polygonal wear discussed above, it induces the polygonal wear and promotes its development.

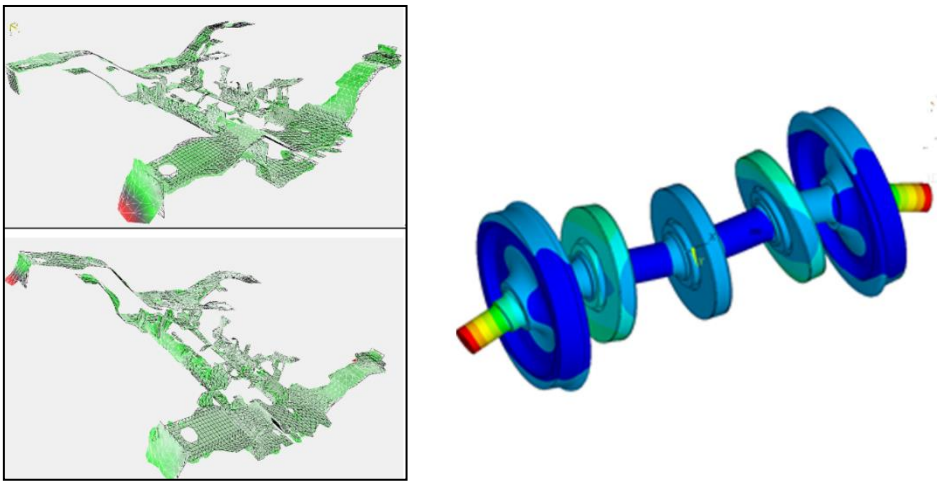

(**a**) (**b**)

Figure 31. (**a**) Two vibration modes of bogie frame at 585 Hz and 595 Hz, (**b**) the fourth-order bending mode of wheelset at 610 Hz.

After the formation mechanism or basic conditions of the polygonal wear were clear, some measures to restrain the development of the polygonal wear were carried out and proved to be very effective. (1) Statistical analysis of the operation field test data showed that the operation speed of the train was changed frequently (frequent stops on a line or frequently changing operation lines), which effectively prevented the development of the polygonal wear [97,99]. This important conclusion was further verified by using the test apparatus shown in Figure 22. The reason for the effectiveness of this measure is simply to break the basic condition for the development of the polygonal wear. Namely, when the train is in operation, the bogie (or wheelset) vibration modes are excited, as shown in Figure 31, and they vibrate at fixed frequencies, which has nothing to do with the change in operation speed. When the operation speed changes frequently, the wavelength of the wheel/rail contact vibration, caused by the excited bogie (or wheelset) mode vibration, changes accordingly. That is, the wavelength of the uneven wear along the wheel circumference changes frequently. So, the basic condition that the wheel rolling circumference be divided exactly by the vibration wavelength is broken. The non-uniform wear with different wavelengths is repeatedly and circularly accumulated on the circumference (or rolling circle) of the wheel, and the final distribution of the total wear along the wheel circumference tends to be uniform. (2) The second effective countermeasure was to apply intelligent trimmers on the treads of high-speed wheels. Using the countermeasure was inspired by tread braking. It was found in the field test that the wheels of the electric locomotives with disc braking systems had serious polygonal wear phenomena of 18-order, as shown in Figure 32a, while the wheels of another kind of electric locomotives with shoe braking system had almost no polygonal wear, as shown in Figure 32b [101].

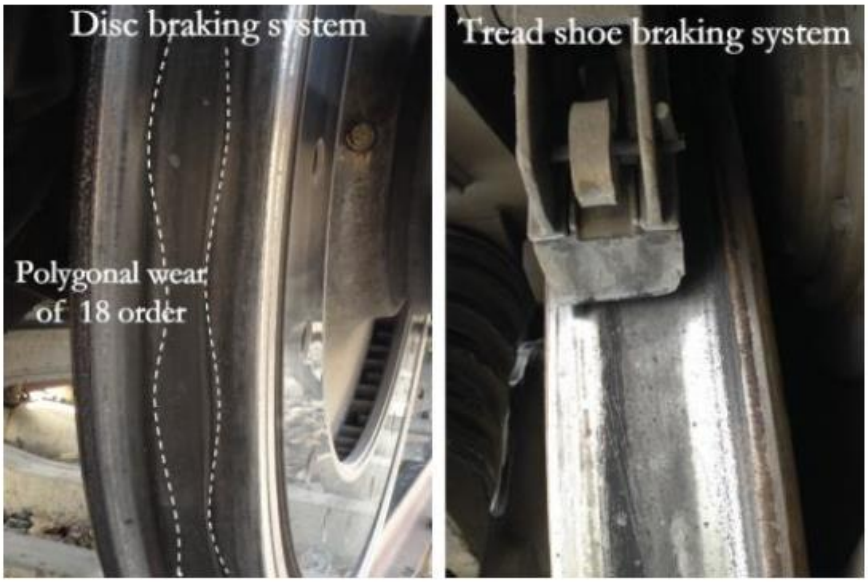

Figure 32. (**a**) Electric locomotive wheel with disc braking system; (**b**) locomotive wheel with brake shoe system.

Later, high-speed trains newly put into operation in China used wheel tread trimmers. Figure 33 shows the site test results. They are the roughness levels along the rolling circle of the wheels of two high-speed trains of the same type. The total operating mileage is about 190,000 km after the re-profiling of wheels. Figure 33a shows the rolling circle roughness levels of the wheels of one train without using tread trimmers. The polygonal wear of 17-order and nine (mainly 17-order) is serious. Figure 33b shows the roughness levels of the wheels of the other train using the trimmers, and shows that the wheels have good roundness. The field test data also prove that the application of the trimmers can not only effectively suppress the development of the polygonal wear, but also effectively suppress the development of wheel hollow wear (as shown in Figure 28) and maintain the stability of the train running for a long time.

The technology and application of wheel tread trimmer need to be further improved. (1) The geometric sizes of the trimmer need to be further optimized. The size of the rolling direction should be more than twice the wavelength of the potential polygonal wear of the wheel, so as to avoid the oscillating of the trimmer along the polygonal wear on the wheel circumference. The wavelength and amplitude of the trimmer oscillating are almost the same as those of the polygonal wear, and fail to effectively eliminate the peaks of the polygonal wear through wear. Its transverse geometry setting is required to effectively suppress the hollow wear at the rolling circle of the wheel caused by the interaction of the wheel and rail during operation (as shown in Figure 28), and efforts should be made to keep the wheel tread with uniform wear and ideal conicity. (2) In order for the trimmer to achieve the function of (1), it needs to be intelligently controlled and intelligently acted, that is, its action effect is related to its action azimuth related to rotating wheel tread, action frequency, action time and pressure amplitude. Even it can sense the wheel tread wear state smartly. These technical considerations also relate to wheel tread wear and damage problems. (3) The last technical issue that needs to be considered is the improvement of the brake shoe material properties of the trimmer. Using the trimmer, excellent material properties can make the functions of (1) and (2) be better guaranteed. The selection of material properties still needs further investigation and analysis of field application.

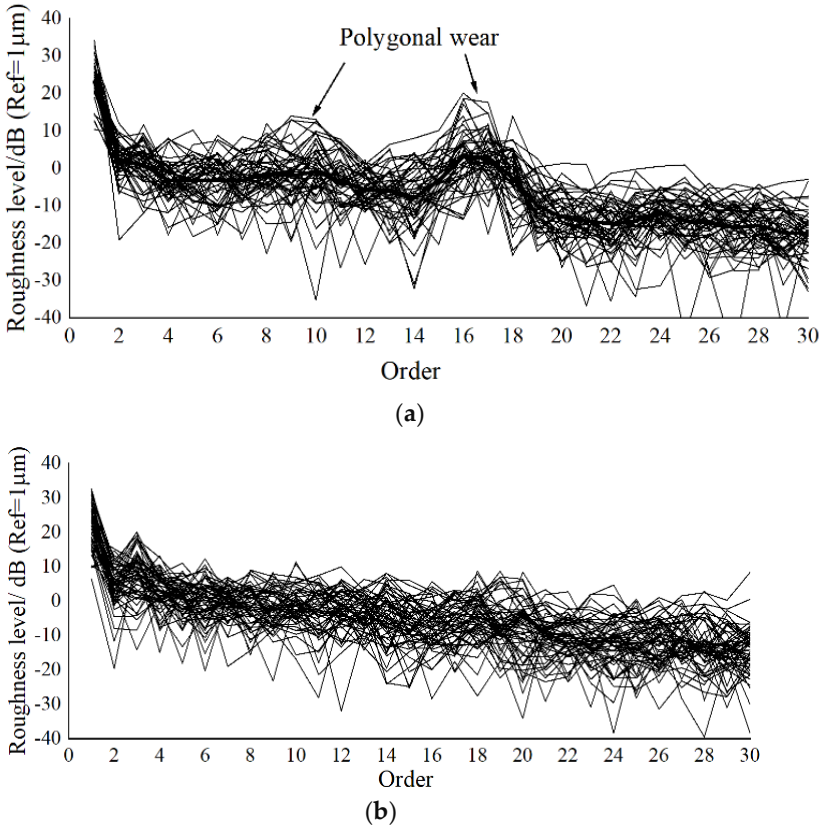

Figure 33. (**a**) High-speed wheels without trimmers; (**b**) high-speed wheels with trimmers.

Rail corrugation occurred on some high-speed railway lines in China shortly after operation. It was not as severe as the existing railway lines (operation speed less than 120 km/h) and urban subways. Rail corrugation occurred in two main environments. (1) Rail corrugation occurred at the small curved tracks entering the train depots. Here, the operation speed is about 30 km/h and the curve radius is about 300 m, as shown in Figure 34. The wavelength of the corrugation on a ballast curved track is about 120 mm and about 100 mm on a slab curved track. The corrugation on the inner rail is more serious than that on the outer rail. The mechanism of its formation is similar to that of the rail corrugation on small curved tracks of urban subways. Because the stick–slip vibration occurs between the wheel and rail when the train is curving, the vibration frequency is mainly determined by the track structure characteristics (that is the lateral track resonance that gets excited), and the wavelength is determined by the stick–slip vibration frequency and the vehicle speed. The countermeasures mainly include lubrication technology, improving transverse stiffness or strengthening stability of the rails at the curved tracks and using the TMD damping system.

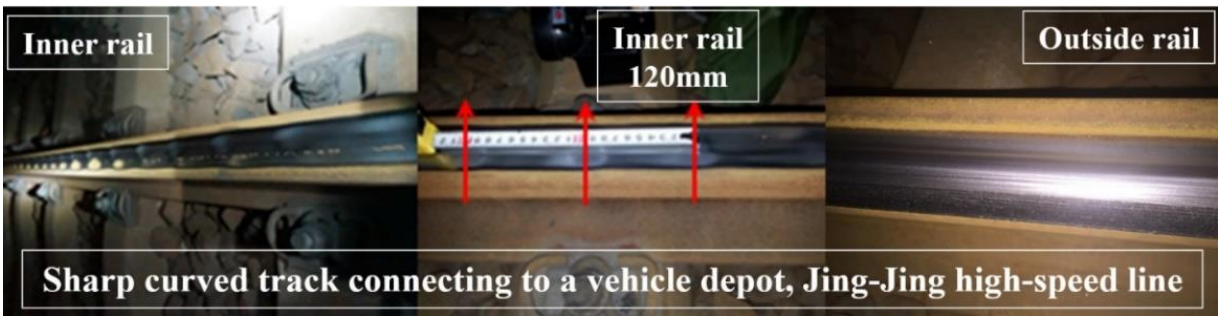

Figure 34. Photos of rail corrugation at a small curved track of high-speed line.

(2) The other environment where rail corrugation occurred is on straight tracks or on large-radii curved tracks (greater than 3000 m). The corrugation state there was slight, as shown in Figure 35a. The corrugation occurred a few months after the rail was ground to remove the decarbonization layer on the top of the new rail. Its main wavelength was about 60–80 mm, and its secondary wavelength was 120–160 mm. Figure 35b shows the photo of the ground rail near the track section shown in Figure 35a. It obviously shows the scratches with the pitch of 60–80 mm caused by the action of grinding train grindstones. This pitch of 60–80 mm was determined by the vertical vibration frequency of the driving unit of the grindstone group and the operation speed of the grinding train. When the train operation speed is 280–300 km/h, the passing frequency of the scratches is about 1000–1100 Hz, which covers the vertical Pin-pin resonance frequency of the track, about 1060 Hz. When a train passed the track with the rail scratches, the vertical Pin-pin resonance of the track was excited, generating the wheel–rail system resonance. The scratches gradually evolved into the corrugation with the same frequency during repeated train passes. So, the scratches similar to those shown in Figure 35b become the origin of the corrugation shown in Figure 35a. Later, the grinding train operation speed was deliberately changed and the pitch of the scratches was changed, so that the passing frequency of the scratches was not close to the vertical Pin-pin resonance frequency of the track. Such doing effectively prevented the evolution of the scratches into rail corrugation. If the vertical working mode frequency of the driving unit of the grindstone group can be changed, the same effect can be achieved.

Figure 35. (**a**) Photo of rail corrugation at a tangent track of a high-speed line; (**b**) photo of the high-speed rail after grinding.

5.2. Rolling Contact Fatigue of High-Speed Wheel–Rail

The rolling contact fatigue state of the wheel–rail of high-speed railways in China is much lighter than that of other wheel–rail transportation systems because of the smooth running and high comfort of high-speed trains, the strict maintenance system of the vehicle and track, the high grade of track lines and the curved tracks with large radii. The wheel and rail materials of China's high-speed railway are mainly made of ER8 and U71MnG steels, respectively, wheel diameter is, respectively, 860 or 920 mm and the CN60 rail is widely used [102]. High-speed wheel–rail rolling contact fatigue can be divided into the following three forms in China.

The first form is a crescent crack on wheel tread, as shown in Figure 36. It was found at the operation sites that the crescent-shaped crack commonly occurred in the middle of the wheel tread and could extend to 5–8 mm deep within 3 months. A large amount of material removal was required to restore the healthy tread. It was also found that with the increase in cutting feed in the damaged wheel repairing, the scope of crescent-shaped cracks on the tread gradually increased. The reason is that the cracks extend downward along a small angle. If the crack is not completely eliminated, the residual crack may lead

to rapid recurrence. For the wheels with general crescent-shaped cracks, it is necessary to cut more than 4 mm to completely eliminate them along the wheel radius, as shown in Figure 36. Crescent-shaped cracks greatly reduce the use life of the wheels. The cause of crescent-shaped cracks was that when the train ran at high speeds, flying foreign matter entered between the wheel–rail contact surfaces and caused material injury on the wheel treads, as shown in Figure 37 [102,103], which evolved into crescent-shaped cracks again in the process of repeated wheel rolling. Laboratory tests were carried out on crescent-shaped-cracked wheelsets to observe and study the law of the crack development. The results of the tests and analysis showed that the crescent-shaped cracks did not extend laterally to the wheel edge and did not extend further in the depth direction, but instead turned to the wheel tread surface, eventually leading to bulk material stripping. It was unlikely to cause the wheel to collapse due to the limited influence depth of wheel–rail contact load, in other words, the lack of driving force for the crescent-shaped crack to extend deeper [103]. The observation and investigation at the operation sites of high-speed trains showed that the crescent-shaped cracks occurred most frequently on the first wheelsets of the head cars of high-speed trains. However, the occurrence frequency of crescent-shaped cracks was not high for all high-speed trains in operation.

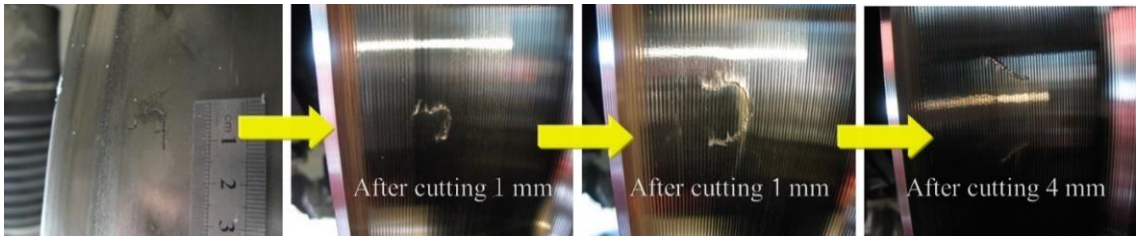

Figure 36. Photos of crescent-shaped crack on wheel tread and state after cutting at different depths in the radius direction.

Figure 37. Photo of crescent-shaped crack.

The second type of rolling contact fatigue of high-speed wheel–rail is the oblique cracks continuously distributed along the wheel rolling circle and within the range of 15–30 mm outside the nominal rolling circle, as shown in Figure 38. The oblique cracks belong to the first type of continuous fatigue in Deuce classification [104] and are the most common rolling contact fatigue [104,105]. The surface hardness of the crack zone is 25–50 HB higher than that of the two sides of the crack zone, which means that the initiation mechanism of the crack should be caused by the accumulation of plastic deformation of the surface material, which is beyond its fatigue or toughness limit [106]. These kinds of fatigue

cracks begin to appear at the operating mileage of about 100,000–150,000 km after wheel re-profiling. In a wheel re-profiling interval (210,000–240,000 km), it can sprout and expand to a depth of 0.25–1.2 mm, but most of them will not develop into stripping. Both bullet train wheels and trailer wheels occurred. Forty-three percent of wheels had such cracks.

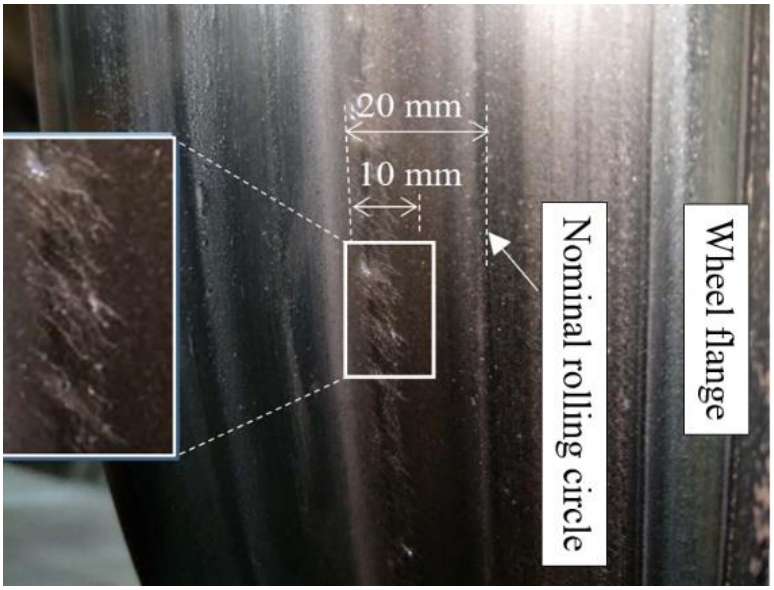

Figure 38. Photo of crescent-shaped crack.

Based on the field measured data of wheel/rail and the establishment of the vehicle-track coupling dynamic model, the numerical simulation of trains passing over curved tracks was carried out. The matching state of wheel/rail profile, rolling contact behavior of wheel/rail and distribution of wheel/rail forces were reproduced, and the relationship mechanism between them and crack initiation and development were analyzed. The numerical results showed that the wheel/rail profile matching was not good (existence of wheel hollow wear) when the trains passed over curved tracks due to the loss of shape, caused by wear and improper design of the rail grinding profile. The contact point was located in the fatigue zone, that is, in the plastic stability and ratchet effect zone, the rolling contact fatigue was very likely to occur. The fatigue crack was the result of the interaction between the wheel and the curve low rail. The longitudinal and transverse creep forces played an important role, and the direction of the cracks was at an angle of about 45 degrees to the rolling direction of the wheel. The most cracks developed in this direction, as shown in Figure 38 [103].

In conclusion, excessive contact stress and creep rate are the key factors leading to the rolling contact fatigue cracks of wheels discussed above, which is consistent with the experimental results in the literature [107]. The following measures can effectively prevent the initiation and development of high-speed wheel fatigue cracks: optimizing the rail profile of curved tracks; frequently and regularly turning around operations of trains on lines with unreasonable distribution of curved tracks, appropriately increasing wheel wear to reduce rolling contact fatigue; optimizing wheel–rail re-profiling/grinding strategy to avoid late stripping and falling blocks; maintaining tracks and vehicles timely; avoiding serious rail corrugation occurring, unreasonable rail bottom slope and track gauge; avoiding the occurrence of the train snake phenomenon.

The third type of rolling contact fatigue of high-speed wheel–rail is that oblique cracks continuously distribute on the rail heads of curved tracks. The crack depth is 0.1– 0.3 mm [102]. The high rails of curved tracks showed oblique cracks in their gauge corner or shoulder. However, the oblique cracks occurred at the low rails, and the severity was lower than that of the high rail cracks. The contact between the rail gauge corner and the wheel rim can be effectively avoided by appropriately reducing the height of

the high rail shoulder near the gauge corner by grinding the high rail. Thus, the rolling contact fatigue of the rail can be suppressed, and the grinding effect can be maintained for 1–2 years.

6. High-Speed Wheel–Rail Noise

High-speed railway noise mainly includes wheel–rail noise, structure vibration noise, air noise, pantograph/catenary noise and operating noise of accessories (such as air conditioning, brake, motor, transformer, gear box, etc.). Previous studies have always believed that when train speed is lower than 300 km/h, wheel/rail noise predominates, and when train speed is higher than 300 km/h, air noise predominates. However, with the improvement of aerodynamic design technology and the manufacturing process of high-speed trains, the current train aerodynamic noise level has gone down significantly and wheel–rail noise level is still dominant [108]. Figure 39 indicates the sound intensity cloud outside an eight marshalling high-speed train operating at 350 km/h. It was obtained using the multi-channel array noise data acquisition and the analysis system based on the Beamforming Sound Source Identification Principle through the field test. Its frequency range is from 500 Hz to 5000 Hz. The Figure shows that the noise is very strong in the two areas outside the train, wheelset/bogie area and pantograph/catenary area. Although the noise intensity in the paragraph/catenary area is a little higher than that in the wheelset/bogie area, a high-speed train with eight marshals has sixteen wheelset/bogie noise sources, but the pantograph/catenary noise source is only one. Therefore, it is believed that the contribution of the wheelset/bogie to the external noise of the train is great when the train is running at high speeds.

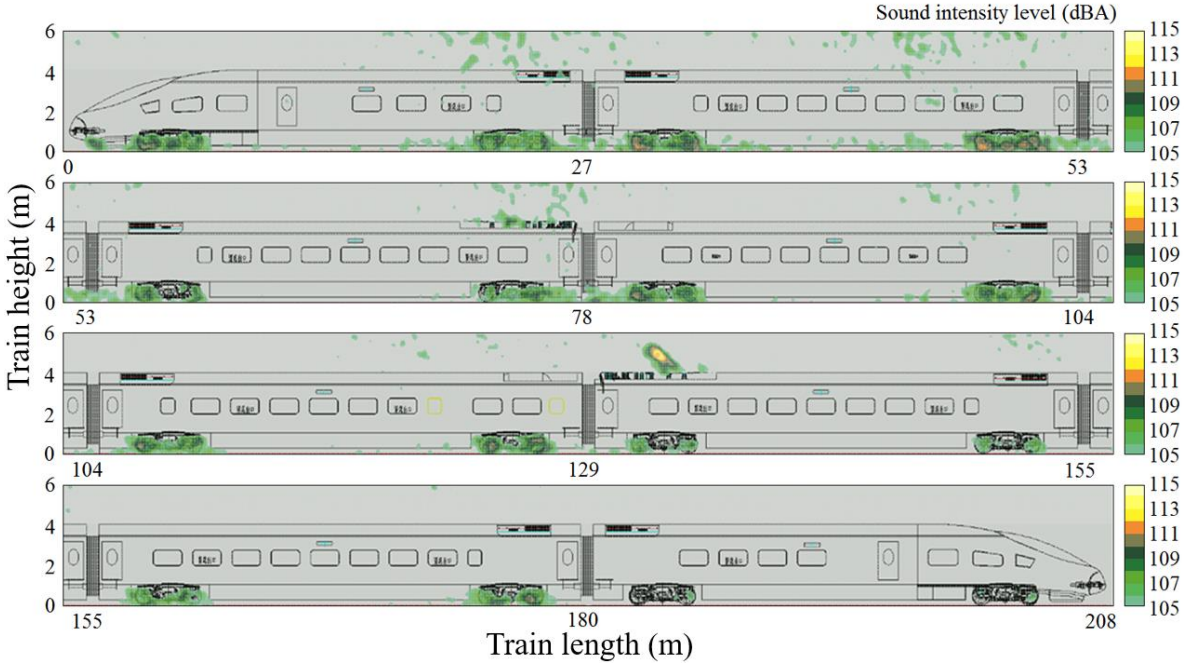

Figure 39. Sound intensity cloud outside an 8 marshalling high-speed train at 350 km/h.

In fact, the strong–noise contribution to the wheel–rail/bogie area is mainly due to the wheel–rail interaction and the aerodynamic action of the bogie complex structure. It is still a challenging problem to analyze and distinguish the proportion of noise contribution to this area and the frequency characteristics in the actual operation of high-speed trains. At present and even for a long time to come, this problem cannot be solved by means of experiments. It is possible to solve this problem by theoretical modeling and numerical simulation in the future [109]. Theoretical modeling and corresponding numerical methods need to be improved from the following aspects. The model of wheel–rail in high-speed rolling contact discussed earlier needs to be further improved. It is believed that the

modeling based on the finite element method is essential because this method can consider more complicated factors affecting wheel–rail rolling contact behavior.

The calculation of flexible deformation of the wheelset and rail structures at high frequencies should abandon the method of linear superposition of modes. In this method, the contribution of each mode to the total vibration of their structures depends on the time-dependent coefficients (called the generalized variables). These coefficients are used to linearly combine the mode shapes of the wheelset and rail under consideration to represent the displacement solution of their structure deformation. They are found by solving the independent linear ordinary differential equations, which are obtained through decoupling the partial differential equations of them. Obviously, the structural characteristics are assumed to be linear. The individual structure modes considered are calculated or experimentally obtained in the free state and under the static, but these modes are not exactly the same as those under the constraints of the actual assembly system and in the service. In addition, it is very difficult to consider and solve the influence of wheelset rotation in mathematical modeling for the existence of higher-frequency modes (2000–8000 Hz) of wheels (pitch-circle and pitch-diameter modes, fan modes, etc.). The high-frequency modes of wheel may be more related to the noise. It is suggested that the differential equations of element motion (element equivalent particle and element equivalent rigid body) and the equilibrium equations of element nodes in a structural medium coordinate system should be established for wheelset/rail structure discretized by using the finite element method in the inertial frame. Through improving the algorithm of the Dyna-3D [42], they are jointly solved. This should be the future research direction of this field, but is also a very challenging problem.

At present, the passive measures to reduce wheel–rail noise mainly include the following aspects: (1) the low noise design of the car body was mainly used to block wheel–rail noise from entering the carriages; (2) reducing wheel–rail irregularity excitation, that is, wheels maintaining higher roundness and rails maintaining smoothness; (3) sound barriers with advanced technology were installed on both sides of high-speed tracks.

7. Conclusions

In the development and operation of high-speed railways in China, the study on the relationship between high-speed wheel and rail have achieved the following results: (1) An elastoplastic theoretical model of three-dimensional high-speed wheel–rail in rolling contact and the corresponding numerical method were developed. Using them, reproduced high-speed wheel/rail rolling contact behavior, taking into account elastoplastic material, high-rate strain effect and various wheel/rail defects. It is the basis and guarantee for recognizing the mechanism of high-speed wheel–rail damage and formulating the wheel–rail maintenance strategy. (2) The establishment of the wheel–rail rolling contact model was extended to consider the influence of high-frequency deformation of wheelset structure and rail structure on wheel–rail behavior and damages, such as the influence on wheel polygonal wear, rail corrugation and wheel–rail noise. (3) The theoretical modeling of high-speed wheel–rail adhesion was further advanced. The influences of actual wheel–rail geometric size, high-speed wheel–rail rolling, elastoplastic roughness contact, oil–water film, oil–water film mixture, temperature and axle weight were taken into account. The high-speed test produced the adhesion curve under the influence of water and roughness, and the test speed reached 450 km/h. The numerical results and experimental results are more reasonable and closer to the reality, which have important application values. (4) The optimal design method of high-speed wheel–rail geometric profile matching was developed. A new high-speed wheel was designed and applied successfully. The design ideas and methods will be extended to the optimization design of urban subway wheel and rail profiles. (5) The characteristics, development law and mechanism of polygonal wear of high-speed train wheels have been basically clarified. The effective measures to restrain the development of the polygonal wear were determined and adopted in a wide range, with good effect. They have been applied to urban subways. (6) Compared with the other

wheel/rail transportation systems (less than 120 km/h), the injury forms of high-speed wheel–rail are less severe. The main reason is the high smoothness of high-speed tracks and high stability of high-speed trains, the large radius curves and the high maintenance level. The causes of these injuries are generally clear.

8. Further Research on Relationship of Wheel and Rail

Although technology, theory and application of the high-speed wheel–rail system achieve some results as described in this paper, the high-speed wheel–rail relationship mentioned in this paper has not been completely solved. It requires long-term in-depth research in the following aspects. (1) Continue to comprehensively track and test at sites, extensively collect the test data and statistically analyze the relationship between wheel/rail in service and dynamic performance of trains running on track lines. It is necessary to completely clarify and classify the mechanism and characteristics of wheel/rail wear and rolling contact fatigue and their main influencing factors at different train speed levels in different regions of China. (2) The wheel–rail profile matching design method proposed in this paper needs to be further improved. The key point of improvement is to develop from the semi-empirical design method to the complete theoretical system. The optimization function can clearly represent the relationship between key influencing factors and design objectives, and the influence of rail wear state can also be reflected in it. The improvement of the vehicle/track dynamic coupling model and wheel/rail wear model is also an important task in improving the wheel–rail profile matching design method. (3) Comprehensively carry out wheel/rail material selection test research, establish wheel/rail material matching database and carry out long-term research on the preparation of new wheel/rail materials. (4) Carry out the technology and application research of intelligent wheel tread trimmer comprehensively and deeply. The working principle and behavior of wheel tread trimmer are similar to those of the wheel tread brake shoe, but its action process is more intelligent. Its objective function is to maintain the ideal conicity of the wheelset and roundness of the wheel in operation, and timely eliminate the micro-cracks and pit wear of the wheel tread. It can effectively make up for the deficiencies of research work (2) and (3) above. (5) Improve the wheel–rail elasto-plastic rolling contact model in the large system environment of vehicle-track coupling. The model should fully consider the following factors influencing the dynamical behavior and rolling contact of wheel/rail system. These factors include wheelset structural deformation, wheelset rotation, contact surface roughness, "third media" between wheel and rail, environment and material defects. The key and difficult points are the modeling of elastoplastic microscopic roughness of wheel–rail contact surface with third media (water, oil, sand, leaves and other pollutants) and the computational efficiency of the model. This part of the research is also the basis and means of the subsequent research works (6) and (7). (6) Continue to carry out theoretical and experimental research on high-speed wheel–rail adhesion and adhesion control technologies. At present, when trains are running at different speeds and under different environments, the problem of low adhesion between wheels and rails often occurs, which leads to large sliding between wheels and rails, thus damaging the wheel–rail contact interface. (7) Carry out in-depth research on the mechanism of high-speed wheel–rail vibration and sound radiation, strengthen the research on low-noise wheel/rail technology application and conduct research on vibration and noise reduction measures. The key factors affecting the vibration and noise of wheel–rail running at different speeds and in different environments are identified, such as the operation speed, the state of the contact surfaces, the structure resonance mode excited, etc.

Funding: This work was funded by the Joint Key Fund Projects (U1134202, U1734201) of the National Natural Science Foundation of China and China Railway Corporation.

Institutional Review Board Statement: Not applicable.

Informed Consent Statement: Not applicable.

Data Availability Statement: Not applicable.

Acknowledgments: Special thanks to my friends and colleagues, Z.F. Wen, S.L. Liang, M.R. Chi, W.W. Wang, X. Zhao, C.Y. Chang, L. Ling, X.X. Xiao, B. Wu, D.B. Cui, G.Q. Tao, S.Q. Zhong, J. Han and Y. Wu. They provided a lot of important information in writing the paper.

Conflicts of Interest: The authors declare no conflict of interest.

References

1. Shen, Z. On the study of high-speed railways and trains. Journal of Vibration. *Meas. Diagn.* **1998**, *18*, 1–7. (In Chinese)
2. Jin, X.; Zhang, X.; Zhang, J.; Sun, L.; Wang, S. Mechanics in performance of wheel-rail. *J. Mech. Strength* **2005**, *27*, 408–418. (In Chinese)
3. Jin, X. Study on Creep Theory of Wheel and Rail System and Its Experimental. Ph.D. Thesis, Southwest Jiaotong University, Chengdu, China, 1999. (In Chinese).
4. Garg, V.K.; Duakkipatti, R.V. *Dynamics of Railway Vehicle Systems*; Academic Press: Orland, CA, USA, 1984.
5. Zhong, S.; Xiao, X.; Wen, Z.; Jin, X. The Effect of first-order bending resonance of wheelset at high speed on wheel-rail contact behavior. *Adv. Mech. Eng.* **2013**, *5*, 296106. [CrossRef]
6. Zhong, S.; Xiong, J.; Xiao, X.; Wen, Z.; Jin, J.A. Effect of the first two wheelset bending modes on wheel-rail contact behavior. *J. Zhejiang Univ. Sci.* **2014**, *15*, 984–1001. [CrossRef]
7. Xiao, X.; Ling, L.; Jin, X. A study of the derailment mechanism of a high speed train due to an earthquake. *Veh. Syst. Dyn.* **2012**, *50*, 449–470. [CrossRef]
8. Ling, L.; Xiao, X.; Xiong, J.; Zhou, L.; Wen, Z.; Jin, X. A 3D model for coupling dynamics analysis of high-speed train/track system. *J. Zhejiang Univ. Sci. A* **2014**, *15*, 964–983. [CrossRef]
9. Zhai, W.; Jin, X.; Wen, Z.; Zhao, X. Wear problem of high-speed wheel/rail systems: Observation, cause, and countermeasures in China. *Appl. Mech. Rev. Nov.* **2020**, *72*, 060801. [CrossRef]
10. Tao, G.; Wen, Z.; Jin, X.; Yang, X. Polygonisation of railway wheels: A critical review. *Rail. Eng. Sci.* **2020**, *28*, 317–345. [CrossRef]
11. Jin, X.; Wen, Z.; Wang, K.; Zhang, W. Effect of a scratch on curved rail on initiation and evolution of rail corrugation. *Tribol. Int.* **2004**, *37*, 385–394. [CrossRef]
12. Ling, L.; Cao, Y.; Xiao, X.; Wen, Z.; Jin, X. Effect of wheel flats on the high-speed wheel/rail contact behavior. *J. China Railw. Soc.* **2015**, *37*, 32–39. (In Chinese)
13. Wen, Z.; Jin, X.; Zhang, W. Contact-impact stress analysis of rail joint region using the dynamic finite element method. *Wear* **2005**, *258*, 1301–1309. [CrossRef]
14. Zhou, X.; Zhao, X.; Han, J.; He, Y.; Wen, Z.; Jin, X. Study on transient rolling noise characteristics of subway wheel with rail corrugation. *J. Mech. Eng.* **2018**, *54*, 196–202. (In Chinese) [CrossRef]
15. Chang, C.; Chen, B.; Liang, H.; Gao, X.; Cai, Y. Experimental study on traction adhesion coefficient between wheel and rail in water condition within 400 km/h speed grade. *China Railw. Sci.* **2021**, *42*, 132–137. (In Chinese)
16. Yang, Z.; Liu, W.; Zhao, G. Research on key mechanics problems in high-speed trains. *Adv. Mech.* **2014**, *44*, 201410. (In Chinese)
17. Carter, F.W. On the action of a locomotive driving wheel. *Proc. R. Soc. Lond.* **1926**, *A112*, 151–157.
18. Ohyama, T. Adhesion characteristics of wheel/rail system and its control at high speeds. *QR RTRI* **1992**, *33*, 19–30.
19. Zhao, X.; Wen, Z.; Wang, H.; Jin, X. Three-dimensional high-speed wheel-rail transient rolling contact finite element model and its application. *J. Mech. Eng.* **2013**, *49*, 1–7. (In Chinese) [CrossRef]
20. Vermeulen, J.K.; Johnson, K.L. Contact of non-spherical bodies transmitting tangential forces. *J. Appl. Mech.* **1964**, *31*, 338–340. [CrossRef]
21. Kalker, J.J. On the Rolling Contact of Two Elastic Bodies in The Presence of Dry Friction. Doctoral Dissertation, The Delft University, Delft, The Netherlands, 1967.
22. Shen, Z.; Hedrick, J.K.; Elkins, J.A. A Comparison of Alternative Creep-Force Models for Rail Vehicles Dynamic Analysis. In Proceedings of the 8th International Symposium on Vehicle System Dynamics, Cambridge, MA, USA, 10–13 August 1983; pp. 591–605.
23. Kalker, J.J. A fast algorithm for the simplified theory of rolling contact. *Veh. Syst. Dyn.* **1982**, *11*, 1–13. [CrossRef]
24. Cai, W.; Wen, Z.; Jin, X.; Zhai, W. Dynamic stress analysis of rail joint with height difference defect using finite element method. *Eng. Fail. Anal.* **2007**, *14*, 1488–1499. [CrossRef]
25. Wen, Z.; Jin, X. Elastic-plastic finite element analysis of repeated, two-dimensional wheel-rail rolling contact under time-dependent load. *Proc. Instn Mech. Engrs Part C J. Mech. Eng. Sci.* **2006**, *220*, 603–613. [CrossRef]
26. Jin, X.; Wu, P.; Wen, Z. Effects of structure elastic deformations of wheelset and track on creep forces of wheel/rail in rolling contact. *Wear* **2002**, *253*, 247–256. [CrossRef]
27. Ogilvy, J.A. Numerical simulation of friction between contact rough surfaces. *J. Phys. D: Appl. Phys.* **1991**, *24*, 2098–2109. [CrossRef]
28. Kalker, J.J. *Three-Dimensional Elastic Bodies in Rolling Contact*; Kluwer Academic Publishers: Dordrecht, The Netherlands, 1990.
29. Zhao, X.; Li, Z. The solution of frictional wheel-rail rolling contact with a 3-D transient finite element model: Validation and error analysis. *Wear* **2011**, *271*, 444–452. [CrossRef]

30. Zhao, X.; Li, Z. A three-dimensional finite element solution of frictional wheel–rail rolling contact in elasto-plasticity. *J. Eng. Tribol.* **2015**, *229*, 86–100. [CrossRef]
31. Jin, X.; Zhang, J. A complementary principle of elastic bodies of arbitrary geometry in rolling contact. *Comput. Struct.* **2001**, *79*, 2635–2644. [CrossRef]
32. Zhang, S.; Li, X.; Wen, Z.; Jin, X. Theory and numerical method of elastic bodies in rolling contact with curve contact area. *Eng. Mechacis* **2013**, *30*, 30–37. (In Chinese) [CrossRef]
33. Zhong, W.; Zhang, H.; Wu, C. *Parametric Variational Principle and Its Application in Engineering*; Science Press: Beijing, China, 1997. (In Chinese)
34. Zhang, J.; Wu, C. Elastic-plastic analysis of wheel-rail contact. *J. China Railw. Soc.* **2000**, *22*, 16–20. (In Chinese)
35. Oden, J.T.; Lin, T.L. On the general rolling contact problem for finite deformations of a viscoelastic cylinder. *Compput. Methods Appl. Mech. Eng.* **1986**, *57*, 297–376. [CrossRef]
36. Padovan, J. Finite element analysis of steady-state transiently moving/rolling nonlinear visco-elastic structures. *Comput. Struct.* **1987**, *27*, 249–257. [CrossRef]
37. Bass, J.M. Three-dimensional finite deformation, rolling contact of a hyper-elastic cylinder: Formulation of the problem and computational results. *Comp. Struct.* **1997**, *26*, 991–1004. [CrossRef]
38. Damme, S.; Nackenhorst, U.; Wetzel, A.; Zastrau, B.W. On the numerical analysis of wheel-rail system in rolling contact. In *Colloquium on System Dynamics and Long-Term Behavior of Railway Vehicles, Track and Subgrade*; Springer: Berlin/Heidelberg, Germany; Stuttgart, Germany, 2002; pp. 155–174.
39. Nackenhorst, U. Zur Berechnung schnell rollender Reifen mit der Finite Element Methode. Doctoral Dissertation, Institut für Mechanik, Universität der Bundeswehr Hamburg, 1992.
40. Nackenhorst, U. On the finite element analysis of steady state rolling contact. In *Contact Mechanics Computational Techniques*; Aliabadi, M.L., Brebbia, C.A., Eds.; Computational Mechanics Publication: Southampton, UK; Boston, MI, USA, 1993; pp. 53–60.
41. Zhao, X. Dynamic Wheel/Rail Rolling Contact at Singular Defects with Application to Squats. Doctoral Dissertation, The Delft University, Delft, The Netherlands, 2012.
42. Zhao, Z.; Wen, Z.; Zhu, M.; Jin, X. A study on high-speed rolling contact between a wheel and a contaminated rail. *Veh. Syst. Dyn.* **2014**, *52*, 1270–1287. [CrossRef]
43. Ling, L.; Xiao, X.; Jin, X. Study on derailment mechanism and safety operation area of high-speed trains under earthquake. *J. Comput. Nonlinear Dyn.* **2012**, *7*, 041001. [CrossRef]
44. Zhao, X.; Liu, C.; Wen, Z.; Jin, X. A study on dynamic stress intensity factors of rail cracks at high speeds by a 3D explicit finite element model of rolling contact. *Wear* **2016**, *366*, 60–70. [CrossRef]
45. Wu, Y.; Han, J.; Liu, J.; Liang, S.; Jin, X. Effect of high-speed train polygonal wheels on wheel/rail contact force and bogie vibration. *Chin. J. Mech. Eng.* **2018**, *54*, 37–46. (In Chinese) [CrossRef]
46. Li, W.; Wang, H.; Wen, Z.; Du, X.; Wu, L.; Li, X.; Jin, X. An investigation into the mechanism of metro rail corrugation using experimental and theoretical methods. *Proc. Inst. Mech. Eng. Part F J. Rail Rapid Transit* **2016**, *230*, 1025–1039. [CrossRef]
47. Han, J.; Zhong, S.; Xiao, X.; Wen, Z.; Zhao, G.; Jin, X. High-speed wheel/rail contact determining method with rotating flexible wheelset and validation under wheel polygon excitation. *Veh. Syst. Dyn.* **2018**, *56*, 1233–1249. [CrossRef]
48. Han, J.; Wang, R.; Wang, D.; Guan, Q.; Zhang, Y.; Xiao, X.; Jin, X. Effect of wheel load on wheel vibration and sound radiation. *Chin. J. Mech. Eng.* **2015**, *28*, 46–54. (In Chinese) [CrossRef]
49. Szolc, T. Medium frequency dynamic investigation of the railway wheelset-track system using a discrete-continuous model. *Arch. Appl. Mech.* **1998**, *65*, 30–45. [CrossRef]
50. Chaar, N. Wheelset Structural Flexibility and Track Flexibility in Vehicle/Track Dynamic Interaction. Doctoral Dissertation, Royal Institute of Technology, Stockholm, Sweden, 2007.
51. Meywerk, M. Polygonalization of railway wheels. *Arch. Appl. Mech.* **1999**, *69*, 105–120. [CrossRef]
52. Szolc, T. *Medium Frequency Dynamic Analysis of Various Designs of the High-Speed Railway Bogie*; Institution of Fundamental Technological Research, Polish Academy of Sciences: Warszawa, Polonia, 2000.
53. Meinders, T. Modeling of a railway wheelset as a rotating elastic multi-body system. *Mach. Dyn. Probl.* **1998**, *20*, 209–219.
54. Meinders, T.; Meinker, P. Rotor dynamics and irregular wear of elastic wheelsets. System dynamics and long-term behaviour of railway vehicles, track and subgrade. *Lect. Notes Appl. Mech.* **2002**, *6*, 133–152.
55. Zhong, S. Study on Vehicle-Track Dynamic System Integrated with High-Speed Rotating Flexible Wheelsets. Ph.D. Thesis, Southwest Jiaotong University, Chengdu, China, 2017. (In Chinese).
56. Zhong, S.; Xiao, X.; Wen, Z.; Jin, X. Effect of wheelset flexibility on wheel–rail contact behavior and a specific coupling of wheel–rail contact to flexible wheelset. *Acta Mech. Sin.* **2016**, *32*, 252–264. [CrossRef]
57. Yang, Z.; Li, Z. A numerical study on waves induced by wheel-rail contact. *Int. J. Mech. Sci.* **2019**, *161–162*, 105069. [CrossRef]
58. Yang, Z.; Deng, X.; Li, Z. Numerical modeling of dynamic frictional rolling contact with an explicit finite element method. *Tribol. Int.* **2019**, *129*, 214–231. [CrossRef]
59. Shen, C.; Deng, X.; Wei, Z.; Dollevoet, R.; Zoeteman, Z.; Li, Z. Comparisons between beam and continuum models for modelling wheel-rail impact at a singular rail surface defect. *Int. J. Mech. Sci.* **2021**, *198*, 106400. [CrossRef]
60. Naeimi, M.; Li, S.; Li, Z.; Wu, J.; Roumen, H.; Petrov, J.S.; Dollevoet, R. Thermomechanical analysis of the wheel-rail contact using a coupled modelling procedure. *Tribol. Int.* **2018**, *117*, 250–260. [CrossRef]

61. Yang, F.; Wei, Z.; Sun, X.; Shen, C.; Núnez, A. Wheel-rail rolling contact behavior induced by both rail surface irregularity and sleeper hanging defects on a high-speed railway line. *Eng. Fail. Anal.* **2021**, *128*, 105604. [CrossRef]
62. Cui, D. Study on Wheel Profile Design Method for High-Speed Train. Doctoral Dissertation, Southwest Jiaotong University, Chengdu, China, 2013. (In Chinese).
63. Jin, X.; Liang, S.; Tao, G.; Cui, D.; Wen, Z. Characteristics, mechanisms, influences and counter measures of high speed wheel/rail wear: Transverse wear of wheel tread. *J. Mech. Eng.* **2018**, *54*, 3–13. (In Chinese) [CrossRef]
64. Zhang, J.; Wen, Z.; Sun, L.; Jin, X. Wheel profile design beaded on rail profile expansion method. *J. Mech. Eng.* **2008**, *44*, 44–49. [CrossRef]
65. Cui, D.; Li, L.; Jin, X. Optimal design of wheel profiles based on weighed wheel/rail gap. *Wear* **2001**, *271*, 218–226. [CrossRef]
66. Shevtsov, I.Y.; Markine, V.L.; Esveld, C. Optimal design of wheel profile for railway vehicles. *Wear* **2005**, *258*, 1022–1030. [CrossRef]
67. Xue, B.; Cui, D.; Li, L.; Du, X.; Wen, Z.; Jin, X. Parallel Inverse Design Method for Wheel Profile. *J. Mech. Eng.* **2013**, *49*, 8–16. (In Chinese) [CrossRef]
68. Li, G.; Zeng, J.; Chi, M.; Song, C.; Gan, F. Study on the improvement of wheel-rail relationship for high speed train. *J. Mech. Eng.* **2018**, *54*, 93–100. (In Chinese) [CrossRef]
69. Zhou, S.; Liang, X.; Li, C.; Zhang, Y. Review on research and application of wheel—Rail hardness matching of high-speed railway at home and abroad. *Railw. Qual. Control.* **2016**, *44*, 33–36. (In Chinese)
70. Wang, W.; Liu, Q.; Zhu, M. Hardness matching behavior of wheel/rail materials. *Tribology* **2013**, *33*, 65–70. (In Chinese)
71. Ohyama, T.; Ohno, K.; Nakano, S. Influence of surface contamination on adhesion force between wheel and rail at high speeds-behavior of adhesion force under the surface contaminated with a small amount of liquid paraffin. *J. Jpn. Soc. Lubr. Eng.* **1989**, *34*, 111–114.
72. Ohyama, T.; Maruyama, H. Traction and slip at high rolling speeds-some experiments under dry friction and water lubrication. In *Proceedings of the Contact Mechanics and Wear of Rail/Wheel Systems, Vancouver, Canada, 6–9 July 1982*; Vancouver, B.C., Ed.; University of Waterloo Press: Waterloo, Canada, 1982; pp. 395–418.
73. Zhang, W.; Chen, J.; Wu, X.; Jin, X. Wheel/rail adhesion and analysis by using full scale roller rig. *Wear* **2002**, *253*, 82–88. [CrossRef]
74. Gallardo-Hernandez, E.A.; Lewis, R. Twin disc assessment of wheel/rail adhesion. *Wear* **2008**, *256*, 1309–1316. [CrossRef]
75. Lewis, R.; Gallardo-Hernandez, E.A.; Hilton, T.; Armitage, T. Effect of oil and water mixtures on adhesion in the wheel/rail contact. *Proc. IMechE Part F J. Rail Rapid Transit* **2009**, *223*, 275–283. [CrossRef]
76. Wang, W.; Zhang, H.; Wang, H.; Liu, Q.; Zhu, M. Study on the adhesion behavior of wheel/rail under oil. water and sanding conditions. *Wear* **2011**, *271*, 2693–2698. [CrossRef]
77. Arias-Cuevas, O. *Low Adhesion in the Wheel-Rail Contact*; Delft University of Technology: Delft, The Netherlands, 2010.
78. Li, Z.; Arias-Cuevas, O.; Lewis, R.; Gallardo-Herna'ndez, E.A. Rolling–sliding laboratory tests of friction modifiers in leaf contaminated wheel–rail contacts. *Tribol. Lett.* **2009**, *33*, 97–109. [CrossRef]
79. Olofsson, U.; Sundvall, K. Influence of leaf, humidity and applied lubrication on friction in the wheel–rail contact: Pin-on-disc experiments. *Proc. Inst. Mech. Eng. Part F J. Rail Rapid Transit* **2004**, *218*, 235–242. [CrossRef]
80. Ohyama, T.; Ohno, K.; Nakano, S. Influence of surface contamination on adhesion force between wheel and rail at higher speeds. *J. Jpn. Soc. Lubr. Eng.* **1988**, *33*, 540–547.
81. Chang, C.; Chen, B.; Cai, Y.; Wang, J. An experimental study of high speed wheel-rail adhesion characteristics in wet condition on full scale roller rig. *Wear* **2019**, *440–441*, 203092. [CrossRef]
82. Ohyama, T. Tribological studies on adhesion phenomena between wheel and rail at high speeds. *Wear* **1991**, *144*, 263–275. [CrossRef]
83. Chen, H.; Ban, T.; Ishida, M.; Nakahara, T. Adhesion between rail/wheel under water lubricated contact. *Wear* **2002**, *253*, 75–81. [CrossRef]
84. Wu, B.; Wen, Z.; Wang, H.; Jin, X. Study on adhesion of wheel and rail under oil pollution. *Eng. Mech.* **2013**, *30*, 392–396. (In Chinese)
85. Wu, B.; Wen, Z.; Wang, H.; Jin, X. Study on factors affecting high-speed wheel-rail adhesion characteristics. *J. China Railw. Soc.* **2013**, *35*, 18–22. (In Chinese)
86. Wu, B.; Wen, Z.; Wang, H.; Jin, X. Numerical analysis method of wheel/rail adhesion under lubrication for high-speed railway. *J. Traffic Transp. Eng.* **2012**, *12*, 41–47. (In Chinese)
87. Chen, H.; Ishida, M.; Nakahara, T. Analysis of adhesion under wet conditions for three-dimensional contact considering surface roughness. *Wear* **2005**, *258*, 1209–1216. [CrossRef]
88. Wu, B. Numerical and Experimental Study on Wheel/Rail Adhesion Characteristics at High Speed. Ph.D. Thesis, Southwest Jiaotong University, Chengdu, China, 2015. (In Chinese).
89. Wu, B.; Wen, Z.; Wang, H.; Jin, X. Numerical Analysis on Wheel/Rail Adhesion under Mixed Contamination of Oil and Water with Surface Roughness. In Proceedings of the 9th International Conference on Contact Mechanics and Wear of Rail/Wheel Systems (CM2012), Chengdu, China, 27–30 August 2012.
90. Chen, H.; Ban, T.; Ishida, M.; Nakahara, T. Effect of water temperature on the adhesion between rail and wheel. *Proc. Inst. Mech. Eng. Part J J. Eng. Tribol.* **2006**, *220*, 571–579. [CrossRef]

91. Zhao, Y.; Maietta, D.; Chang, L. An asperity micro-contact model incorporating the transition from elastic deformation to fully elastic deformation to fully plastic flow. *J. Tribol.* **2000**, *122*, 86–93. [CrossRef]
92. Wu, B.; Xiao, G.; An, B.; Wu, T.; Sheng, Q. Numerical study of wheel/rail dynamic interactions for high-speed rail vehicles under low adhesion conditions during traction. *Eng. Fail. Anal.* **2022**, *137*, 106266. [CrossRef]
93. Wu, B.; Yang, Y.; Xiao, G. A Transient Three-Dimensional Wheel/Rail Adhesion Model under Interfacial Contamination Considering Starvation and Surface Roughness. In Proceedings of the 12th International Conference on Contact Mechanics and Wear of Rail/Wheel Systems (CM2022), Melbourne, Australia, 4–7 September 2022.
94. Yang, Z.; Zhang, P.; Moraal, J.; Li, Z. An experimental study on the effects of friction modifiers on wheel–rail dynamic interactions with various angles of attack. *Rail. Eng. Sci.* **2022**, *30*, 360–382. [CrossRef]
95. Jin, X.; Wu, Y.; Liang, S.; Wen, Z.; Wu, X.; Wang, P. Characteristics, mechanism, influences and countermeasures of polygonal wear of high-speed train wheels. *J. Mech. Eng.* **2020**, *56*, 118–136. (In Chinese)
96. Zhang, J.; Han, G.X.; Xiao, X.B.; Wang, R.Q.; Zhao, Y.; Jin, X.S. Influence of wheel polygonal wear on interior noise of high-speed trains. *J. Zhejiang Univ. SCIENCE A (Appl. Phys. Eng.)* **2014**, *15*, 1002–1018. [CrossRef]
97. Wu, Y.; Jin, X.; Cai, W.; Han, J.; Xiao, X. Key Factors of the initiation and development of polygonal wear in the wheels of a high-speed train. *Appl. Sci.* **2020**, *10*, 5880. [CrossRef]
98. Wu, Y.; Du, X.; Zhang, H.; Wen, Z.; Jin, X. Experimental analysis of the mechanism of high-order polygonal wear of wheels of a high-speed train. *J. Zhejiang Univ. Sci. A* **2017**, *18*, 579–592. [CrossRef]
99. Wu, Y.; Wang, J.; Liu, M.; Jin, X.; Hu, X.; Xiao, X.; Wen, Z. Polygonal wear mechanism of high speed wheels based on full-size wheel-rail roller test rig. *Wear* **2022**, *494*, 204234. [CrossRef]
100. Wu, Y.; Han, J.; Zuo, Q.; Jin, X.; Liang, Y. Effect of rail corrugation on initiation and development of polygonal wear. *J. Mech. Eng.* **2020**, *56*, 198–208. (In Chinese)
101. Tao, G.; Wang, L.; Wen, Z.; Guan, Q.; Jin, X. Experimental investigation into the mechanism of the polygonal wear of electric locomotive wheels. *Veh. Syst. Dyn.* **2018**, *56*, 883–899. [CrossRef]
102. Zhao, X.; Wen, Z.; Wang, H.; Tao, G.; Jin, X. Research progress on wheel/rail rolling contact fatigue of rail transit in China. *J. Traffic Transp. Eng.* **2021**, *21*, 1–35. (In Chinese)
103. Zhao, X.; An, B.; Zhao, X.; Wen, Z.; Jin, X. Local rolling contact fatigue and indentations on high-speed railway wheels: Observations and numerical simulations. *Int. J. Fatigue* **2017**, *103*, 5–16. [CrossRef]
104. Deuce, R. *Wheel Tread Damage-an Elementary Guide*; Bombardier Transportation Gmbh: Netphen, Germany, 2007.
105. Ekberg, A.; Kabo, E.; Karttunen, K.; Lindqvist, B.; Lundén, R.; Nordmark, T.; Olovsson, J.; Salomonsson, O.; Vernersson, T. Identifying the root causes of damage on the wheels of heavy haul locomotives and its mitigation. *Proc. Inst. Mech. Eng. Part F J. Rail Rapid Transit* **2014**, *228*, 663–672. [CrossRef]
106. Wang, Y.; Lu, C.; Zhao, X.; Wen, Z. Rolling contact fatigue of Chinese high speed wheels: Observations and simulations. *J. Mech. Eng.* **2018**, *54*, 150–157. (In Chinese) [CrossRef]
107. Ekberg, A.; Kabo, E.; Andersson, H. An engineering model for prediction of RCF of railway wheels. *Fatigue Fract. Eng. Mater. Struct.* **2002**, *25*, 899–909. [CrossRef]
108. Zhang, S. Identification and control of noise mechanism of high-speed train at 350km/h. *China Railw. Sci.* **2009**, *30*, 86–90. (In Chinese) [CrossRef]
109. Han, J.; Zhong, S.; Zhou, X.; Xiao, X.; Zhao, G.; Jin, X. Time-domain model for wheel-rail noise analysis at high operation speed. *J. Zhejiang Univ. Sci. A* **2017**, *18*, 593–602. [CrossRef]